THESIS FOR THE DEGREE OF DOCTOR OF PHILOSOPHY

Bits and Pieces for the Nuclear Puzzle

Exploring light exotic nuclei with radioactive ion beams

RONJA M. A. THIES

Department of Physics
CHALMERS UNIVERSITY OF TECHNOLOGY
Gothenburg, Sweden 2016

Bits and Pieces for the Nuclear Puzzle
Exploring light exotic nuclei with radioactive ion beams
RONJA M. A. THIES
ISBN 978-91-7597-426-2

Doktorsavhandlingar vid Chalmers tekniska högskola
Ny serie nr. 4107
ISSN 0346-718X

Department of Physics
Chalmers University of Technology
SE-412 96 Gothenburg
Sweden
Telephone: +46 (0)31-772 1000

Cover:
Artistic version of the plot of the measured one-proton-x-neutron (with $x \leq 5$) removal cross sections for carbon isotopes. The original version of the plot with legend and axis labels is found in Fig. 4a of Paper I.

Chalmers Reproservice
Gothenburg, Sweden 2016

Bits and Pieces for the Nuclear Puzzle
Exploring light exotic nuclei with radioactive ion beams
RONJA M. A. THIES
Department of Physics
Chalmers University of Technology

Abstract

Atomic nuclei are a fascinating case of many-body systems governed by quantum behaviour. This fact and the complex nuclear interaction are reasons why there is not yet a complete theory describing all atomic nuclei. Both experimental and theoretical efforts are needed to change this situation. Stable nuclei have been studied extensively, but more exotic nuclear systems are not yet well understood, and it is there where we expect to find improvements to our understanding of the complex nuclear interaction.
Beams of light exotic nuclei have become accessible for experiments, and together with recent advances in detection systems, they open up possibilities for studying extreme nuclear systems up to and beyond the driplines, into the continuum. Experiments with light exotic beams deliver important data from extreme nuclear systems, which help to improve the description of atomic nuclei in general. This thesis is focused on light neutron-rich nuclei, and studies them in different ways. Proton-removal cross sections from boron and carbon isotopes are used to test the reaction model ABRABLA07. The agreement is surprisingly good, but the need for a better understanding of the induced excitation energy is demonstrated. Unbound nuclei beyond the dripline are produced via proton-knock-out reactions and studied. The data on the oxygen isotopes agree well with 3N-interaction shell-model calculations. The rare (βp) decay channel is observed in the halo nucleus ^{11}Be. Nuclear reactions also play an important role in astrophysics and the question of how heavy elements are generated in our universe. Coulomb dissociation cross sections can be used to determine astrophysically important (n,γ) rates. Measured cross sections for ^{20,21}N and ^{17}C provide improved input for r-process network calculations.

Keywords:
Neutron-rich nuclei, Radioactive Beams, R^{3}B, GSI, FAIR, ISOLDE

List of Publications

This thesis is based on the following appended papers:

I **R. Thies**, A. Heinz, T. Adachi, Y. Aksyutina, J. Alcantara-Núñes, S. Altstadt, H. Alvarez-Pol, N. Ashwood, T. Aumann, V. Avdeichikov, M. Barr, S. Beceiro-Novo, D. Bemmerer, J. Benlliure, C. A. Bertulani, K. Boretzky, M. Borge, G. Burgunder, M. Caamano, C. Caesar, E. Casarejos, W. Catford, J. Cederkäll, S. Chakraborty, M. Chartier, L. V. Chulkov, D. Cortina-Gil, R. Crespo, U. Datta, P. Díaz Fernández, I. Dillmann, Z. Elekes, J. Enders, O. Ershova, A. Estradé, F. Farinon, L. M. Fraile, M. Freer, M. Freudenberger, H. O. U. Fynbo, D. Galaviz, H. Geissel, R. Gernhäuser, K. Göbel, P. Golubev, D. Gonzalez Diaz, J. Hagdahl, T. Heftrich, M. Heil, M. Heine, A. Henriques, M. Holl, G. Ickert, A. Ignatov, B. Jakobsson, H. T. Johansson, B. Jonson, N. Kalantar-Nayestanaki, R. Kanungo, R. Knöbel, T. Kröll, R. Krücken, J. Kurcewicz, N. Kurz, M. Labiche, C. Langer, T. Le Bleis, R. Lemmon, O. Lepyoshkina, S. Lindberg, J. Machado, J. Marganiec, V. Maroussov, M. Mostazo, A. Movsesyan, A. Najafi, T. Nilsson, C. Nociforo, V. Panin, S. Paschalis, A. Perea, M. Petri, S. Pietri, R. Plag, A. Prochazka, A. Rahaman, G. Rastrepina, R. Reifarth, G. Ribeiro, M. Ricciardi, C. Rigollet, K. Riisager, M. Röder, D. Rossi, J. Sanchez del Rio, D. Savran, H. Scheit, H. Simon, O. Sorlin, V. Stoica, B. Streicher, J. T. Taylor, O. Tengblad, S. Terashima, Y. Togano, E. Uberseder, J. Van de Walle, P. Velho, V. Volkov, A. Wagner, F. Wamers, H. Weick, M. Weigand, C. Wheldon, G. Wilson, C. Wimmer, J. Winfield, P. Woods, D. Yakorev, M. V. Zhukov, A. Zilges and K. Zuber. "Systematic investigation of projectile fragmentation using beams of unstable B and C isotopes". In: *Phys. Rev. C* 93 (5 May 2016), p. 054601. DOI: 10.1103/PhysRevC.93.054601. arXiv: 1603.00323 [nucl-ex]

II K. Riisager, O. Forstner, M. Borge, J. Briz, M. Carmona-Gallardo, L. Fraile, H. Fynbo, T. Giles, A. Gottberg, A. Heinz, J. Johansen, B. Jonson, J. Kurcewicz, M. Lund, T. Nilsson, G. Nyman, E. Rapisarda, P. Steier, O. Tengblad, **R. Thies** and S. Winkler. "^{11}B(βp), a quasi-free neutron de-

cay?" In: *Phys. Lett. B* 732 (2014), pp. 305–308. DOI: 10.1016/j.physletb.2014.03.062

III C. Caesar, J. Simonis, T. Adachi, Y. Aksyutina, J. Alcantara, S. Altstadt, H. Alvarez-Pol, N. Ashwood, T. Aumann, V. Avdeichikov, M. Barr, S. Beceiro, D. Bemmerer, J. Benlliure, C. A. Bertulani, K. Boretzky, M. J. G. Borge, G. Burgunder, M. Caamano, E. Casarejos, W. Catford, J. Cederkäll, S. Chakraborty, M. Chartier, L. Chulkov, D. Cortina-Gil, U. Datta Pramanik, P. Diaz Fernandez, I. Dillmann, Z. Elekes, J. Enders, O. Ershova, A. Estrade, F. Farinon, L. Fraile, M. Freer, M. Freudenberger, H. O. U. Fynbo, D. Galaviz, H. Geissel, R. Gernhäuser, P. Golubev, D. Gonzalez Diaz, J. Hagdahl, T. Heftrich, M. Heil, M. Heine, A. Heinz, A. Henriques, M. Holl, J. D. Holt, G. Ickert, A. Ignatov, B. Jakobsson, H. T. Johansson, B. Jonson, N. Kalantar- Nayestanaki, R. Kanungo, A. Kelic-Heil, R. Knöbel, T. Kröll, R. Krücken, J. Kurcewicz, M. Labiche, C. Langer, T. Le Bleis, R. Lemmon, O. Lepyoshkina, S. Lindberg, J. Machado, J. Marganiec, V. Maroussov, J. Menéndez, M. Mostazo, A. Movsesyan, A. Najafi, T. Nilsson, C. Nociforo, V. Panin, A. Perea, S. Pietri, R. Plag, A. Prochazka, A. Rahaman, G. Rastrepina, R. Reifarth, G. Ribeiro, M. V. Ricciardi, C. Rigollet, K. Riisager, M. Röder, D. Rossi, J. Sanchez del Rio, D. Savran, H. Scheit, A. Schwenk, H. Simon, O. Sorlin, V. Stoica, B. Streicher, J. Taylor, O. Tengblad, S. Terashima, **R. Thies**, Y. Togano, E. Uberseder, J. Van de Walle, P. Velho, V. Volkov, A. Wagner, F. Wamers, H. Weick, M. Weigand, C. Wheldon, G. Wilson, C. Wimmer, J. S. Winfield, P. Woods, D. Yakorev, M. V. Zhukov, A. Zilges, M. Zoric and K. Zuber. "Beyond the neutron drip line: The unbound oxygen isotopes ^{25}O and ^{26}O". in: *Phys. Rev. C* 88 (3 Sept. 2013), p. 034313. DOI: 10.1103/PhysRevC.88.034313

IV M. Röder, T. Adachi, Y. Aksyutina, J. Alcantara, S. Altstadt, H. Alvarez-Pol, N. Ashwood, L. Atar, T. Aumann, V. Avdeichikov, M. Barr, S. Beceiro, D. Bemmerer, J. Benlliure, C. Bertulani, K. Boretzky, M. J. G. Borge, G. Burgunder, M. Caamaño, C. Caesar, E. Casarejos, W. Catford, J. Cederkäll, S. Chakraborty, M. Chartier, L. Chulkov, D. Cortina-Gil, R. Crespo, U. Datta Pramanik, P. Diaz-Fernandez, I. Dillmann, Z. Elekes, J. Enders, O. Ershova, A. Estrade, F. Farinon, L. M. Fraile, M. Freer, M. Freudenberger, H. Fynbo, D. Galaviz, H. Geissel, R. Gernhäuser, K. Göbel, P. Golubev, D. Gonzalez Diaz, J. Hagdahl, T. Heftrich, M. Heil, M. Heine, A. Heinz, A. Henriques, M. Holl, G. Ickert, A. Ignatov, B. Jakobsson, H. Johansson, B. Jonson, N. Kalantar-Nayestanaki, R. Kanungo, A. Kelic-Heil, R. Knöbel, T. Kröll, R. Krücken, J. Kurcewicz, N. Kurz, M. Labiche, C. Langer, T. Le Bleis, R. Lemmon, O. Lepyoshkina, S. Lindberg, J. Machado, J. Marganiec, M. Mostazo Caro, A. Movsesyan, M. A. Najafi, T. Nilsson, C. Nociforo, V. Panin, S. Paschalis, A. Perea, M. Petri, S. Pietri, R. Plag, A. Prochazka, M. A. Rahaman, G. Rastrepina, R. Reifarth, G. Ribeiro, M. V.

Ricciardi, C. Rigollet, K. Riisager, D. Rossi, J. Sanchez del Rio Saez, D. Savran, H. Scheit, H. Simon, O. Sorlin, V. Stoica, B. Streicher, J. Taylor, O. Tengblad, S. Terashima, **R. Thies**, Y. Togano, E. Uberseder, J. Van de Walle, P. Velho, V. Volkov, A. Wagner, F. Wamers, H. Weick, M. Weigand, C. Wheldon, G. Wilson, C. Wimmer, J. S. Winfield, P. Woods, D. Yakorev, M. Zhukov, A. Zilges and K. Zuber. "Coulomb dissociation of ^{20,21}N". in: *Phys. Rev. C* 93 (6 June 2016), p. 065807. DOI: 10.1103/PhysRevC.93.065807.

V M. Heine, T. Adachi, Y. Aksyutina, J. Alcantara, S. Altstadt, H. Alvarez-Pol, N. Ashwood, T. Aumann, V. Avdeichikov, M. Barr, S. Beceiro, D. Bemmerer, J. Benlliure, C. A. Bertulani, K. Boretzky, M. J. G. Borge, G. Burgunder, M. Caamano, C. Caesar, E. Casarejos, W. Catford, J. Cederkäll, S. Chakraborty, M. Chartier, L. Chulkov, D. Cortina-Gil, U. D. Pramanik, P. D. Fernandez, I. Dillmann, Z. Elekes, J. Enders, O. Ershova, A. Estrade, F. Farinon, L. M. Fraile, M. Freer, M. Freudenberger, H. O. U. Fynbo, D. Galaviz, H. Geissel, R. Gernhäuser, P. Golubev, D. G. Diaz, J. Hagdahl, T. Heftrich, M. Heil, A. Heinz, A. Henriques, M. Holl, J. D. Holt, G. Ickert, A. Ignatov, B. Jakobsson, H. T. Johansson, B. Jonson, N. Kalantar-Nayestanaki, R. Kanungo, A. Kélic-Heil, R. Knöbel, T. Kröll, R. Krücken, J. Kurcewicz, M. Labiche, C. Langer, T. L. Bleis, R. Lemmon, O. Lepyoshkina, S. Lindberg, J. Machado, J. Marganiec, V. Maroussov, J. Menéndez, M. Mostazo, A. Movsesyan, A. Najafi, T. Neff, T. Nilsson, C. Nociforo, V. Panin, A. Perea, S. Pietri, R. Plag, A. Prochazka, A. Rahaman, G. Rastrepina, R. Reifarth, G. Ribeiro, M. V. Ricciardi, C. Rigollet, K. Riisager, M. Röder, D. Rossi, J. S. del Rio, D. Savran, H. Scheit, A. Schwenk, H. Simon, J. Simonis, O. Sorlin, V. Stoica, B. Streicher, J. Taylor, O. Tengblad, S. Terashima, **R. Thies**, Y. Togano, S. Typel, E. Uberseder, J. V. de Walle, P. Velho, V. Volkov, A. Wagner, F. Wamers, H. Weick, M. Weigand, C. Wheldon, G. Wilson, C. Wimmer, J. S. Winfield, P. Woods, M.-R. Wu, D. Yakorev, M. Zhukov, A. Zilges, M. Zoric and K. Zuber. "Measurement of the Neutron-Capture Rate of ^{17}C for the R-process Nucleosynthesis". In: *submitted to Phys. Rev. C* (2016). arXiv: 1604.05832 [nucl-ex]

Contribution Report

Common contributions to Papers I, III, IV, V

I have taken part in the full experiment and in the preparation period immediately before the experiment. I have developed a new, time-dependent calibration method for and calibrated the Crystal Ball detector (XB). I have contributed to debugging and improvements of the analysis software of the collaboration, LAND02, e.g. by implementing the add-back routine for the XB detector (after Paper III was published), and implementing a workaround for the partial failure of the ToF detector at the FRS. I have contributed to debugging and improvements of the tracking software LAND/R^{3}B TRACKER. The contributions to the analysis and tracking software generally benefit all experiments performed with the LAND/R^{3}B setup and the future R^{3}B, not only the experiment or papers concerned in this thesis.

Contributions to Paper I

I have calibrated all detectors which were used in the analysis except the SST, POS, PSP and the ToF detector at the FRS (the workaround is used). I have done all analysis of the experimental data (using the above-mentioned software for unpacking and tracking). I have run the ABRABLA07 and EPAX3 model calculations and implemented the tested modifications. The ideas to the modifications were developed in discussion between me and my co-supervisor, Andreas Heinz. I wrote and submitted the manuscript (with suggestions from supervisors and collaborators).

Contributions to Paper II

I have taken part in both the preparatory and production experiments and their preparations. I have read the manuscript and given suggestions for improvements.

Common contributions to Papers III, IV, V

I have read the manuscripts and given suggestions for improvements.

Contents

1. Introduction

The size of human beings is on the length-scale of a meter. We are made of cells, and those are made of molecules. Molecules consist of atoms, which are composed of electrons surrounding atomic nuclei. The atomic nucleus has a size of a few fm, 10^{-15} m. To give a feeling for this length scale, Table 1.1 lists different length scales and examples of objects with that approximate size at intervals of 10^3 (the scaling factor between a meter and a millimeter). The atomic nucleus is built of neutrons and protons, held together by the nuclear interaction, a residual of the strong force, which binds quarks together to neutrons and protons (and also to other hadrons). How do the neutrons and protons hold together to form atomic nuclei? This is the key question we want to answer in nuclear physics.

The answer to this question is not only interesting on the scale of the atomic nucleus. This answer also governs the life of stars and how stars and supernova work, as it is in these huge (approximately 10^9 m large) objects that elements[1] are formed. The energy freed by the formation of heavier elements is causing the stars to shine. Understanding and being able to describe the nuclear interaction will also improve our understanding of these huge objects out in the Universe.

Even though we, at present, know almost 4000 isotopes (of which only around 300 do not decay), there exists no theory which can describe all nuclei and all their relevant properties. Nuclear physicists around the world work in order to improve this situation.

In this thesis I present experiments with beams of light neutron-rich nuclei

[1] Hydrogen, (not all) helium and some amount of lithium have been formed in the big-bang.

m	mm	μm	nm	pm	fm
humans	grain of sand	cells	molecules	atoms*	atomic nucleus

Table 1.1: Length scales and examples of objects of the corresponding size. Each length scale is 0.001 of the length scale to its left. $\star$ This is very approximate; atoms are a little larger: rather 10 - 100 pm in radius.

which aim at improving our understanding of atomic nuclei. These experiments, focused on one part of the nuclear landscape, cover a broad range of different aspects of nuclear physics: we measure reaction cross sections and try to improve model calculations with these. We prove the existence of a predicted decay channel and try to understand the dynamics of this decay. Unbound nuclear systems are created and studied to improve our understanding of nuclei at the limit of existence. Extending to astrophysics we experimentally determine neutron capture cross sections, which are important for the understanding of the formation of the elements our world is made of in astrophysical objects (like stars and supernova explosions).

Structure of the thesis

This chapter gives an introduction to nuclear physics in general, explains radioactive ion beam production and why light neutron-rich nuclei – the core of this work – are particularly interesting. The second chapter introduces experimental methods and observables of interest for this work. Ch. 3 gives an overview of the radioactive ion beam facilities and experimental setups used. Chs. 4 - 6 deal with the specific physics cases of the appended papers. In Ch. 4 we look at $1pxn$ removal cross sections for neutron-rich boron and carbon beams at relativistic energies. We also explore how well model calculations can reproduce these cross sections. Ch. 5 summarizes results from nuclei at the neutron drip line and beyond. Unbound ^{25,26}O and ^{16}B are studied and a previously unobserved decay channel from ^{11}Be is observed. Ch. 6 presents results from Coulomb dissociation of neutron-rich carbon and nitrogen isotopes, which are of interest for astrophysical production rates of heavier elements.
Finally, Ch. 7 discusses the impact of the results in this thesis, and Ch. 8 presents an outlook.

1.1 Introduction to Nuclear Physics

Atoms consist of electrons surrounding the nucleus which is made of protons and neutrons. Though protons and neutrons are about 2000 times heavier than the electrons, they cluster together in a tight core: the diameter of the electron cloud of an atom is about 10000 times larger than its nucleus [1, 2]. Neutrons interact only by the strong and weak (nuclear) forces[2]. But since protons are electrically charged, there are two forces governing the interactions of nucleons (protons and neutrons), the electromagnetic and the strong nuclear force. These two forces determine whether a certain combination of

[2]In first approximation. From their internal quark structure they have a non-vanishing magnetic moment - which means they also interact electromagnetically.

protons and neutrons can exist in a bound state, forming a nucleus. They can only form a nucleus if the potential energy of the individual nucleons alone is larger than the potential energy of them forming a (bound) nucleus. The difference of these energies is the binding energy, and represents the work required to take all the nucleons apart again. It is often more convenient to regard the energy it takes to remove a single proton or neutron, which is called the separation energy.

The weak force turns protons into neutrons and vice versa, so bound nuclei can decay by turning protons into neutrons and the other way around (called β-decay). In general, if the binding energy can be increased by β-decay, the nucleus will do so (eventually). There can be more than one isotope which is stable against β-decay per isobar[3] (but only for even mass number, A). Those nuclei, which do not decay, are situated in the so-called valley of β-stability, and form the centerpiece of the atoms we encounter in our everyday lives. For light nuclei, the valley of β-stability approximately corresponds to nuclei having the same amount of protons (Z) as neutrons (N), while for heavier nuclei the valley moves to more neutron-rich nuclei as protons repel each other electromagnetically, decreasing the binding energy. (See e.g. the interactive nuclear chart and other comprehensive tables at the NNDC [3].)

Starting in the valley of β-stability, adding protons or neutrons to a nucleus turns it into a more and more exotic[4] nucleus, which has shorter and shorter[5] β-decay half-lives until the dripline is reached. The driplines mark where it is not possible to add a further proton (proton dripline) or a neutron (neutron dripline) to a nucleus such that it is bound. This is like adding balls to a ball-net: at one point the net is full and no further ball(s) can be added. The tricky aspect in nuclear physics is that the balls inside the net determine how large the net is, and which type of balls are allowed into it (protons or neutrons).

The first microscopic theory to successfully describe the properties of atomic nuclei is the nuclear shell model [4], developed by Maria Goeppert-Mayer around 1950. It predicts magic numbers, spins and magnetic moments of the at that time known, mostly stable, nuclei correctly, excluding odd-odd[6] nuclei[7]. Predicting the properties of stable nuclei and those close to shell closures

[3] An isobar is the ensemble of all nuclei with the same amount of nucleons A.

[4] Nuclear systems which are far away from stability and difficult to produce and study and decays that have only been observed a few times are called exotic. Which nuclei and decays are considered exotic might change over time as new facilities and detectors allow us to push the borders of difficult. This is very much in line with "Yesterday's sensation is today's calibration." (R. P. Feynman) "...and tomorrow's background." (V. L. Telegdi).

[5] This describes the general trend. The details of the nuclear interaction and decay are more intricate and thus the behavior is more complicated.

[6] The term odd-odd indicates that the number of protons and the number of neutrons is odd. If both N and Z were even one would have stated even-even nucleus.

[7] Goeppert-Mayer states that the coupling between the spins of the two odd nucleons is not known, but that it evidently not couples to zero. The single-particle orbitals for the odd nucleons are correctly assigned by the shell model, for those five nuclei which had been measured.

very well, this model lays the foundation of our understanding of the nuclear interaction and governs the nomenclature in nuclear physics.
The shell model is limited since it uses a mean-field potential instead of the potential each single nucleon experiences due to its interactions with all the other nucleons in the nucleus. Away from shell closures shell model calculations become computationally extremely challenging, since there are many valence nucleons and residual interactions allow for configuration mixing. These problems can be amended by introducing effective residual interactions in a phenomenological way – but that limits the predictive power of the model [5].
Since the development of the shell model, nuclear theory has advanced a lot. Newer approaches are e.g. based on the nucleon-nucleon interaction and effective field theories (see e.g. Ref. [6]). All nuclear physics theories have so far one thing in common: they are successful in certain areas of the nuclear landscape or applicable for certain nuclear physics questions, but limited in other ones. Difficulties arise from the underlying complexity of the problem: an atomic nucleus is a many-body system with quantum behaviour and the interaction is a complex remnant of the strong force.

1.2 Radioactive Ion Beam production

The limitation imposed by the use of beams consisting of stable (or long-lived) isotopes hampered advances in nuclear physics experiments for a long time. Nuclear physics has made a large step forward with the development of radioactive ion beam facilities in the late 1980s. Nowadays, we can create more and more isotopes, and prepare beams of almost all known. This opened possibilities to study isotopes further and further away from beta-stability and for a quest of new features, which give us clues about what needs to be improved in our understanding of nuclei, and how.
Producing a beam of a certain isotope is not at all a straightforward process and requires large accelerator facilities. A recent review [7] summarizes RIB facilities and techniques. There are two basic approaches to produce a beam of a certain isotope, and those are introduced in the following.

1.2.1 The ISOL approach

The Isotope Separator OnLine (ISOL) technique uses beams of stable light particles (often protons) at high kinetic energies impinging on a thick heavy target (e.g. uranium-carbide) to produce all kinds of lighter isotopes via fragmentation, fission and spallation reactions of the target nuclei. A detailed, comprehensive description of this technique can be found in e.g. Ref. [8]. The target is usually heated such that the produced isotopes can diffuse out quicker and more easily. The isotopes need to be ionized so that they can be acceler-

ated, separated and guided to the experiment. Typical techniques are surface, plasma, and resonant laser ionization. By using photons from a laser whose energy is specifically tuned to resonant excitation of the electrons, it is possible to more efficiently and more selectively ionize the isotope of interest as compared to using surface or plasma ionization [9]. Laser ionization can be used in principle for all elements and would be preferential because of its selectivity, but efficient ionization schemes are not available for all elements. In surface ionization the target and ionization cavity are heated such that atoms ionize on contact [10]. Surface ionization is also very selective in terms of the element number, and thus very suitable, but has the limitation that the ionization potential needs to be smaller than 7 eV or the electron affinity larger than 1.5 eV. Volatile elements can typically not be ionized by any of the two former methods. They are ionized by plasma ionization (through collisions with electrons) [11], which is capable of ionizing all isotopes, but lacks elemental selectivity. For a summary of which element can be best ionized with which technique see Ref. [7].
After ionization the ions are accelerated, most often using a static potential (of typically several tens of kV). After the acceleration, the ion trajectories are bent using a magnet, thus enabling the separation of the different isotopes according to their magnetic rigidity, and thus mass, selecting the isotope(s) of interest [8]. The beam can now be guided directly to an experimental setup, it can be further accelerated (to at maximum a few MeV/nucleon at present facilities), or it can be purified using e.g. an ion trap [7].
This method of beam generation has a few challenges. Due to the need of diffusion and ionization, chemistry plays an important role in which isotopes can be extracted, while at the same time providing an important selectivity. Furthermore, this process takes time, so the lifetimes of the isotope of interest needs to be at least about 10 ms. Due to the low kinetic energy, molecules and different charge states can cause impurities in the beam.
ISOL-type facilities around the world are e.g. CERN-ISOLDE (Switzerland), JYFL (Finland), TRIUMF-ISAC (Canada), and GANIL-SPIRAL (France).

1.2.2 The in-flight approach

The in-flight approach uses fragmentation (and fission) of a heavy beam impinging on a light target (often beryllium) to produce beams of exotic isotopes. The primary beam can have energies of a few tens of MeV/nucleon up to several GeV/nucleon, depending on what the accelerator can deliver. See Table 1.2 for an overview of major in-flight facilities and the maximum magnetic rigidity of their beams, and Ref. [12] for a detailed introduction. Due to the high kinetic energies and the reaction mechanism, the resulting fragments are moving at almost incoming beam velocity. Due to that, no chemistry is in-

max Bρ [Tm]	Facility	Country
3.2	GANIL	France
3.5	NSCL	USA
8	FRIB*	USA
9	RIBF	Japan
18	GSI	Germany
20†	FAIR*	Germany

Table 1.2: In-flight facilities around the world and their maximum magnetic rigidity. $\star$ This facility is still under construction. † The accelerator of this facility is designed to accelerate beams with up to 100 Tm rigidity, the separator can only work with (secondary beams) up to a maximum of 20 Tm.

volved in extracting the ions of interest from the target. Since they move at almost incoming beam velocity the ions do not need post-acceleration after production. The isotopes of interest are selected via bending magnet(s), slits, and degraders, and then guided to the experimental area [7]. The shortest possible lifetime of the produced isotopes depends on the time of flight between production target and experimental setup, which is typically a few hundred nanoseconds in the laboratory frame of reference [12]. The shorter transport time in comparison to the ISOL method enables studies of less stable beams, but also introduces impurities by isomeric states[8]. In comparison to ISOL beams, the in-flight beams have a higher emittance, requiring tracking of the incoming beam. Though in-flight beams are often fully stripped for light to medium mass ions, this is not always the case for heavy ions. For these, charge-states can pose difficulties in beam identification.

1.3 Light Exotic Nuclei

With the tools to produce exotic nuclei at hand, these have been the focus in recent years. This thesis presents experimental results on light neutron-rich nuclei, and a few reasons why this region is particularly interesting are presented in the following.
Exotic atomic nuclei can test extreme cases that highlight specific properties of the nuclear interaction and, as already hinted at in Sec. 1.1, this is where the biggest improvements of our understanding of the nuclear interaction are expected. The nuclei in the vicinity of the driplines (on both sides) are the most extreme cases possible. While the proton dripline is already quite well established, reaching the dripline is more difficult on the neutron-rich side. The

[8]This of course also allows to study these isomeric states.

neutron dripline is only well established experimentally up to oxygen [13], and though experimentally observed ^{31}F, ^{34}Ne and ^{37}Na are expected to be drip line nuclei, this is not yet experimentally established [14]. Nuclei at and beyond the dripline (and its location) give important clues about the transition from bound nuclei to the continuum.

In this "transition zone", phenomena which are only found near the driplines occur. One important phenomenon are halos in nuclei, first discovered in ^{11}Li by Tanihata *et al.* [15] and interpreted by Hansen and Jonson [16]. A nuclear halo develops when a part of the wave function(s) of certain nucleon(s) extends too far outside of the core into the classically forbidden region. This can happen for low angular momentum states if they are not strongly bound [17]. The most common halos consist of one or two of either neutrons or protons. Other systems exist, like ^{8}He, but it is unclear whether this nucleus should be regarded as a nucleus with a four neutron halo or as a nucleus with a neutron skin [17]. Two-nucleon halo nuclei are typically borromean, meaning that their subsystems of nucleon-core and neutron-neutron or proton-proton are unbound [18].

Another interesting phenomenon which has been observed for light neutron-rich nuclei, is the disappearance of traditional shell closures (magic numbers) and appearance of new shell closures. N = 8 is not magic for He, Li and Be [19], while it is for nuclei closer to stability. This is explained by the $2s_{1/2}$ orbital being lower in energy than the $1p_{1/2}$ orbital for these nuclei, which is not the case for the isotopes closer to stability. In other words the $2s_{1/2}$ orbital intrudes into the p-shell [19].

Also the neutron-rich oxygen isotopes are intriguing: ^{24}O appears to be doubly magic [20], thus having a shell closure at N=16, while it also is the most neutron-rich bound oxygen isotope. This introduces a new shell closure which is not present for nuclei in the valley of β-stability. ^{28}O was expected to be bound and doubly magic, but is unbound [21] and thus the dripline for oxygen is at A=24, while it extends to (at least [14]) A=31 for fluorine. This is called the oxygen anomaly. The nucleus is also remarkable as it is one of very few doubly magic dripline nuclei known so far. (Other candidates are ^{48}Ni and ^{100}Sn.)

Also for other nuclei, namely neutron-rich Ne, Na, and Mg nuclei, the traditional shell closure at N = 20 is not present, and this area is called the "island of inversion" [22]. Deformation was identified early on as a cause [23, 24], these first interpretations suggested the intrusion of the $f_{7/2}$ orbital. Recent reviews [25, 26] refer to shape coexistence as the reason for deformation and disappearance of shell closures.

Another interesting phenomenon is beta-delayed particle emission which occurs close to the driplines (though not restricted to light nuclei). The β decay of the mother nucleus feeds excited states above particle threshold in the primary daughter nucleus, which subsequently emits the particle(s). Known

particle emissions are proton-, neutron-, deuteron-, triton, alpha-particle-, and even two-neutron-, two-proton-emission and multi-particle decays [27]. Beta-delayed decays can proceed via specific states in the primary daughter, as described above, but can also proceed directly to the continuum. These decays offer therefore an opportunity to study the coupling to the continuum.
The phenomena described above are exotic behaviours which theories of nuclear physics need to be able to explain and predict. Light exotic nuclei exhibit fascinating properties, which new theories can benchmark against, while still being computationally accessible to theories that describe nuclei based on bare nucleon-nucleon forces, due to the few nucleons involved in each nucleus.

2. Observables and Experimental Tools

There exists a broad range of experimental observables which can be extracted in nuclear physics experiments. In order to learn about a certain aspect of atomic nuclei one needs to choose a suitable combination of experimental method and observable. The following section summarizes selected observables relevant in (but not restricted to) the mass region addressed in this thesis.
The combination of experimental method and observable(s) to be extracted imposes requirements on the experimental setup to be used. Different nuclear reactions and how they can be used to probe certain aspects of nuclear structure are introduced in the second section of this chapter. For completeness, the last section introduces the concept of inverse kinematics, which is important for Papers I, III, IV, and V.

2.1 Observables

Observables can be defined in different ways. A rigorous definition of an observable is that the expectation value(s) of its corresponding hermitian operator do not change. I would like to use a more relaxed definition in this work in order to be able to differentiate between measured quantities we observe in our detectors, and quantities we reconstruct from these measurements and use for comparison and input to model calculations. The latter are called observables in this work.
Measured quantities are e.g. energy-loss, time-of-flight, and position. From these, we can reconstruct particle properties such as momentum, particle type, etc. With that information, selection of reaction channel and reaction reconstruction is possible and the quantities, subsequently called observables, can be extracted. The observables used in this work are model independent (and thus compatible with the strict definition) unless indicated otherwise. Interpretation of the observables generally needs model-dependent input.

Cross Sections

The cross section of a nuclear reaction is a measure for the probability of the reaction channel when projectile and target nuclei scatter. This probability depends on the following parameters: kinetic energy of the nuclei, impact parameter, polarization and, of course, on which isotopes collide. The kinetic energy, polarization and isotopes can be experimentally controlled, while the impact parameter cannot.
The cross section (σ) is calculated from the number of ions that underwent the reaction divided by the total number of incoming ions and the number of ions in the target per area.

$$\sigma = \frac{N_{reac}}{N_{in} \cdot N_{target,cm^{-2}}} \tag{2.1}$$

One can measure total cross sections, but also energy- or angle-dependent differential cross sections.
Total interaction cross sections can be used to deduce the matter radius of nuclei - that way halo nuclei were discovered [15]. Scanning energy-ranges, and thus measuring energy-dependent differential cross sections, one can for example find resonances (energies for which the cross section is enhanced), which can be relevant for e.g. astrophysical reaction rates.
A few of the other observables which are introduced (the relative energy, momentum distributions, fractional energies) are in principle also cross section measurements, the cross section is here measured as a function of the other observable.

Relative Energy

When unbound nuclei or (excited) states above the particle emission threshold are populated, the relative energy is an interesting observable, which gives information about the energy of the system before particle emission. Through a fit of the relative energy spectrum with Breit-Wigner resonance functions [28], one can also deduce the orbital angular momentum of the emitted particle(s). The relative energy is reconstructed from the difference of the invariant masses of the system before and after the emission, subtracting the excitation energy emitted via γ-rays. It can therefore be calculated from the four-momenta of the outgoing fragment and the emitted particle(s). (The complete set of them can only be measured in inverse kinematics at high enough energies, which requires a relativistic approach.) For one-particle emission the relative energy is calculated, as derived from the invariant mass, according to:

$$E_{fp} = \sqrt{M_f^2 + M_p^2 - 2 \cdot \gamma_f \cdot \gamma_p \left(1 - \beta_f \cdot \beta_p\right)} - (M_i) \tag{2.2}$$

with M denoting the restmass, β the velocity in units of c and γ the Lorentz factor of the fragment (f) and emitted particle (p). M_i denotes the rest mass of the ground state of the decaying system; for unbound nuclei this is equal to $(M_f + M_p)$.

Excitation Energy

In a similar manner to the reconstruction of the relative energy, it is also possible to reconstruct the total excitation energy from the invariant mass. That requires detection of all emitted γ-quanta and the reconstruction of their energy in the rest-frame of the emitter. One can then calculate the total excitation energy of a system by summing the relative energy (if particles were emitted) and the energy emitted by γ-emission. This can be used to obtain information on the state the fragment is in after, e.g., particle emission.

Transversal Momentum

Nucleons in different single-particle-states have different momenta: d-state nucleons have higher momenta than p-state nucleons, which in turn have higher momenta than s-state nucleons. This can be understood from Heisenberg's uncertainty principle, and the spatial extension of the single particle orbitals for the different states. Single particle orbitals with higher angular momentum are more localized, as the extension and form of the orbitals are governed by Spherical Harmonics. When removing one of the nucleons via knockout, and, to a good approximation, not interacting with the rest of the nucleus, the width of the transversal momentum distribution of the remaining fragment depends on the single-particle state of the removed nucleon only. The momentum parallel to the beam axis holds the same information and, depending on the accuracy of the measurement, it is beneficial to analyse either the parallel or the transversal momentum (since usually one has better experimental resolution). More information can be found in e.g. Ref. [29].
In order to extract the single-particle-state (or the different components if the states are not pure), the distribution needs to be compared to theoretical estimates of widths for the different states. To calculate the expected distributions, a typical approach uses the Glauber model together with the sudden approximation and either the Monte-Carlo black disc approach or the eikonal optical potential. For further reading on these types of calculations, see e.g. Ref. [30].

Profile Function

When using knockout reactions of nucleons in the halo of borromean nuclei, it is possible to correlate the information of transverse momentum with the rel-

ative energy into a profile function, as done in Ref. [31]. The profile function is the width of the transverse momentum distribution as a function of relative energy, i.e. for the events in small relative energy intervals the width of the transverse momentum is determined, and plotted as a function of the relative energy. As explained above, the transverse momentum carries information about the angular momentum of the knocked-out nucleon, while the resonances in the relative energy can be assigned to different angular momenta of the unbound nucleon.
By comparing to theoretical calculations of the variance for removal from states with different angular momenta, it is possible learn more about the population of single-particle states by both nucleons (those removed and those subsequently unbound) simultaneously. Therefore it is possible to reconstruct the initial population of single-particle states by the two halo nucleons.

β-decay half-lives

Half-lives of β-decaying nuclei can serve to improve the understanding of the structure of mother and daughter nuclei, and as important input to astrophysics calculations of heavy element production.
Generally the half-lives of decays to certain states in the daughter nucleus are of interest, which can be translated into branching ratios of these decay paths and vice versa. From that one can calculate the matrix element of the transition, which in turn gives information about the structure of the mother and daughter nuclei and the decay process.
The equation describing half-lives of β-decay is:

$$ft_{1/2} = \frac{K}{g_V^2 B_F + g_A^2 B_{GT}} \tag{2.3}$$

with B_F and B_{GT} being the matrix elements for Fermi and Gamow-Teller decay respectively, f the phase space of the decay and $K/g_V^2 = 6144.2(16)$ s and $g_A/g_V = -1.2694(28)$ [32], g_A denoting the axial and g_V the vector coupling constants, respectively.
For nuclear astrophysics, additionally to total half-lives, the detailed information of branching ratios are important as decays to certain (excited) states might be of importance due to resonant behaviour, long half-lives or allow for particle emission breaking out of r- or p-process paths.
β-spectroscopy, where energies of the outgoing particles are measured, is an even more powerful tool, as it allows for a better reconstruction of decays and the involved states.

2.2 Inverse kinematics

Due to the nature of the radioactive ion production, and the short half-lives involved, it is not possible to machine a target out of highly unstable nuclei[1], thus they have to be used as the beam.
Traditionally nuclear physics experiments were performed by scattering a light beam (i.e. of electrons, protons or α-particles) off the heavier nucleus. Since this is not possible for exotic isotopes, the heavier nucleus is used as beam, scattering off the lighter target. This is called inverse kinematics and brings several advantages additionally to making scattering experiments with exotic nuclei possible. The biggest advantage is that the heavy nucleus, which is the subject of study, leaves the target and can be detected (provided that the beam energy is high and the target thickness small enough), significantly improving the possibilities of reaction reconstruction. This is not usually possible for direct kinematics, and the reaction channel has to be deduced from the other outgoing particles in that case [2].
Inverse kinematics is not suitable for all kinds of measurements. For example, recoils in the low-energy region cannot be measured.

2.3 Nuclear reactions as experimental tools

Though it is not possible to control what kind of nuclear reaction takes place when two nuclei interact, it is possible to tune the experimental conditions such that the desired reaction has a high probability. The beam energy and the target type and material are the main parameters. The different reactions (combined with the right observables) reveal different properties of nuclei. The following discussions assume that the reaction takes place in inverse kinematics, i.e. the beam is the nucleus to be studied and the target is the nucleus used as probe.

Knockout Reactions and Quasi-free Scattering

Knockout reactions are reactions in which one or two nucleons are removed from the nucleus under study due to a direct nuclear interaction between the nucleon(s) and the probe nucleus. Knockout reactions can be used with several different goals and are usually performed at beam energies of 100 -

[1] There exist targets made of long-lived unstable nuclei such as tritium targets. They are complicated to handle, though.

[2] It might seem that Coulomb excitation at relativistic energies, does not fulfill the criterion of lighter target than beam, since the target material is usually lead or a similar high-Z material. The reaction of interest is though the nucleon scattering with a photon in the Coulomb-field of the target nuclei, and the photon is the lighter particle.

1000 MeV/nucleon and rather light targets like hydrogen, beryllium or carbon. They proceed in such a way that the probe nucleus only interacts with the nucleon(s) it knocks out from the beam nucleus, and thus leaves the rest of the nucleus unperturbed (except that nucleons are missing). This defines the lower border of energy range given above: the kinetic energy needs to be large enough such that the de Broglie wavelength of the colliding nucleons is on the scale of single nucleons and not on the scale of the nucleus. This requirement is met for roughly 100 MeV/nucleon (2.8 fm). Knockout reactions offer therefore the opportunity to study the properties of the nucleon in the nucleus it was removed from, by studying e.g. the transverse or parallel momentum of the remaining fragment. These reactions can also be used to populate excited states in the fragment in order to study them by γ-spectroscopy. The creation of unbound nuclei is another important use of knockout reactions. Those, and any excited states that allow for particle emission can be studied by relative energy (and γ-spectroscopy), which give information about the properties of the state(s) of the emitted nucleon before emission.
A special case of knock-out reactions are quasi-free (QF) knockout reactions. Quasi-free means that the target-nucleus interaction is so unlikely that, in inverse kinematics, the target penetrates into the beam nucleus and can probe deeply-bound states. This is achieved as follows: The target nuclei should be as small as possible, thus protons are an ideal choice. The beam energy needs to be tuned such that the nucleon-nucleon cross section is as small as possible, rendering the likelihood of the proton to interact with a nucleon independent of the position of the nucleon in the nucleus. For p-p collisions the smallest cross section is in the range of 200 MeV/nucleon to 2000 MeV/nucleon while for p-n collisions the cross section decreases with increasing beam energy and is constant above about 700 MeV/nucleon [33].
This reaction type has the advantage that it is possible to probe also nucleons in deeply bound states [34]. Especially the generation of unbound nuclei on the neutron-rich side benefits if the knockout reaction proceeds in a quasi-free manner, since there usually a deeply bound proton needs to be removed to create an unbound nucleus.

Fragmentation Reactions

Fragmentation reactions are less selective than knockout reactions and common for larger projectiles and targets. Usually one can still divide the nuclei of projectile and target each into participants and spectators, but typically more nucleons are removed. In a geometric picture, the whole overlap zone between beam and target is abraded from both nuclei. This generally leaves the projectile-fragment in a highly excited state, which decays by particle-evaporation and γ-emission.
Fragmentation reactions are used to generate secondary beams using the in-

flight method (described in Sec. 1.2). They are also used to study the resulting fragment via γ-spectroscopy. Paper I reports measured fragmentation cross sections and uses them to test fragmentation models.

Coulomb Excitation and Dissociation

In Coulomb excitation or dissociation the nucleus interacts with the electromagnetic field of a target nucleus, and gets excited by that interaction. In order to achieve a significant cross section in comparison to nuclear interactions, the electrostatic potential needs to be strong. Thus, targets with high Z, like gold or lead are preferred. Beam energies range from a few MeV/nucleon for "safe Coulomb excitation" to a few GeV/nucleon for relativistic beams.
Coulomb excitation is usually combined with γ-spectroscopy to study the states the beam nucleus is excited to. When the nucleus is excited to states which allow for particle emission, that process is called Coulomb dissociation. The measurement of (γ,p) and (γ,n) cross sections is of astrophysical importance, as these can be transformed, using the principle of detailed balance, to cross sections for (p,γ) and (n,γ) reactions. Those reactions are relevant for astrophysical proton and neutron capture processes. The latter reaction has been measured for nitrogen and carbon isotopes and is reported in Papers IV and V.

3. RIB facilities and experimental setups

The experiments forming the basis of the papers pertinent to this thesis were performed at two RIB facilities, CERN-ISOLDE and GSI Helmholtz Centre for Heavy Ion Research. This chapter describes the facilities and experimental setups used.

3.1 CERN-ISOLDE

The ISOLDE (Isotope Separator On Line DEvice) facility is located at CERN and uses proton beams with kinetic energies of 1 GeV or 1.4 GeV provided by the Proton Synchrotron Booster (PSB)[1] [36]. As its name indicates, it uses the ISOL method to create and separate radioactive isotopes. ISOLDE has two independent separators (see Fig. 3.1), the General Purpose Separator, GPS, and the High Resolution Separator, HRS. Each of them has its own target station. To ionize the ions produced in the target, surface, plasma, and laser ionization (c.f. Sec. 1.2.1) can be used at ISOLDE. The acceleration in both separator branches can be chosen to be 30 to 60 keV. The GPS uses one 70° magnet to separate the ions and has a mass resolving power ($M/\Delta M$) of 2400 [36]. Two beam lines, both leading to collection stations, can only be reached via the GPS (c.f. Fig. 3.1). The HRS, as its name indicates, achieves a better mass resolving power of up to 15000. This is achieved by two magnets with different bending directions and electrostatic elements for higher order beam corrections [36]. After passing through the HRS, the beam enters an RF cooler (with bunching capabilities), the RFQ, which focuses the beam from having an emittance of around 30 π mm mrad to an emittance of 3 π mm mrad [37].
Downstream of the cooler and the two collector beam lines at the GPS the beam lines from the GPS and the HRS are joined, and all subsequent beam

[1] Since 1992 it is situated there, the earlier ISOLDE facility received beams from the Synchro-Cyclotron at CERN.

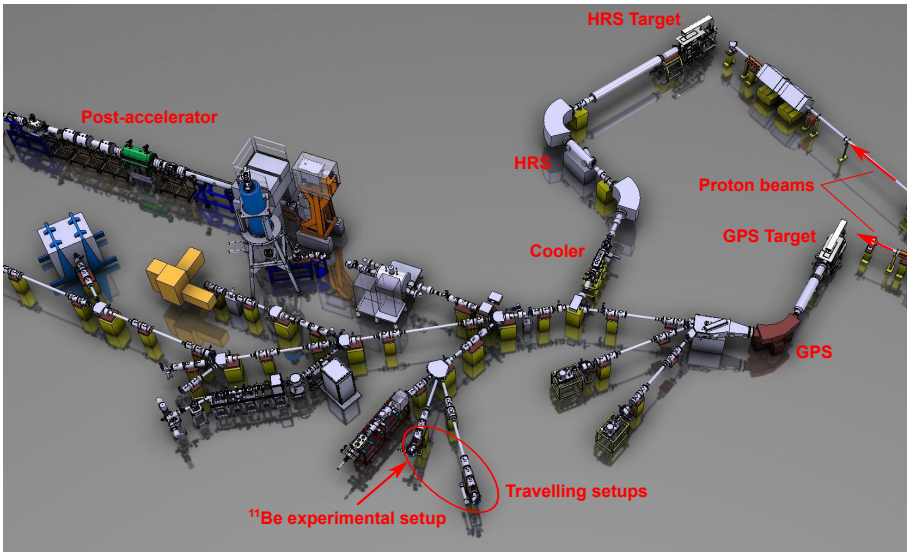

Figure 3.1: Sketch of the ISOLDE facility, modified from Ref. [35]. Radioactive beams can be created via the General Purpose Separator (GPS), or with the High Resolution Separator (HRS). The experiment reported here uses the HRS separator. The experimental setup used was located at the second arm for "travelling setups" as indicated. For details see text.

lines and experiments can be reached by beams from both separators. Steering is done via electrostatic kickers and quadrupoles.
ISOLDE has a post-accelerator called REX, which is currently upgraded from being able to accelerate ions up to 3 MeV/nucleon to being able to accelerate ions up to 10 MeV/nucleon, which is expected to be achieved in 2018[2] [38].
Most experiments at ISOLDE are stationary installed setups (in most small modifications are possible). There are two beam lines at ISOLDE for so called "travelling setups", at one of which the setup used in Paper II was installed, see Fig. 3.1.

3.1.1 The setup for collection of ^{11}Be

The experiment was performed to determine the branching ratio of ^{11}Be(βp) and is divided into two parts: the collection of ^{11}Be and the measurement of ^{10}Be. The latter was performed with the accelerator mass spectrometer at the Vienna Environmental Research Accelerator, VERA, a dedicated machine for

[2]The facility is running again after a longer break, and the remaining upgrades are performed during the shut down periods in winter.

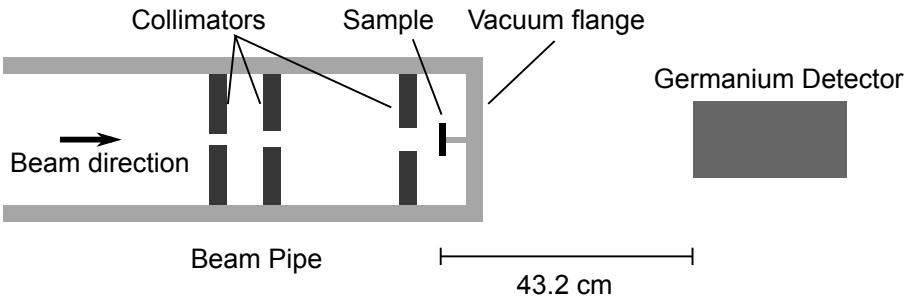

Figure 3.2: Schematic drawing of the experimental setup for the collection of ^{11}Be at CERN-ISOLDE (not to scale). The distance between Ge-detector and implantation plate (sample) is 43.2 cm.

AMS (Accelerator Mass Spectrometry). More information about VERA can be found in Ref. [39]. The setup for the collection is what is considered "experimental setup" in this context. The beam of ^{11}Be was generated by bombarding a uranium-carbide target with 1.4 GeV protons. The created radioactive species were ionized using laser ionization with the RILIS ion source [40], which provided the first selection (in element number). The HRS was used to select ^{11}Be. With its resolution it is no problem to separate ^{11}Be from possible contaminants like ^{11}Li, as also shown in the paper. With the selection done by the HRS, the rest of the setup has two main tasks: to collect ^{11}Be and to count how many ions were implanted in the collector plate.
The dedicated setup, shown in Fig. 3.2, therefore consists of three circular collimators and the collector plate, each of which have a current reading, and a co-axial germanium-detector. The current reading of the collimators enables on-line monitoring of beam focus and steering. The current reading from the collector plate, made of copper, delivers an on-line estimate of the number of implanted ions. The germanium detector is used to detect γ emission associated with the β-decay of ^{11}Be from which the total amount of implanted ^{11}Be can be determined.
The collimator and collector pieces were designed specifically for that experiment, while the germanium-detector is a standard detector available at the ISOLDE facility.

3.2 GSI Helmholtz Centre for Heavy Ion Research

Exotic beams at the GSI Helmholtz Centre for Heavy Ion Research in Darmstadt, Germany are created using the in-flight technique at its fragment separator FRS [41].

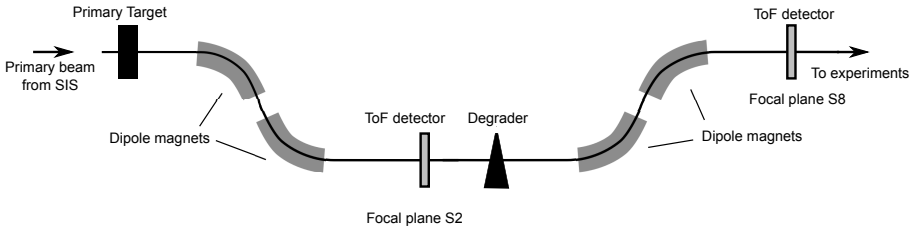

Figure 3.3: Schematic drawing of the fragment separator FRS at GSI. Beam steering and monitoring devices except time-of-flight (ToF) detectors are not indicated. For details see text.

The stable beams at GSI are generated from plasma ion sources[3] [42] and accelerated up to 20 % of the speed of light in a linear accelerator called UNILAC. From that they are injected to the SIS18, a synchrotron able to accelerate the beam up to magnetic rigidities of 18 Tm, which can be up to 90 % of the speed of light, depending on the ion. This primary beam is then guided to the FRS, the fragment separator at GSI, where production and selection of the exotic ions takes place. Impinging onto a production target[4] as indicated in Fig. 3.3, the beam collides with the nuclei in it. Fragmentation, knock-out and, if the beam is heavy enough, fission reactions create a wide range of lighter isotopes. From these, the isotopes of interest need to be selected.
The selection uses the $B\rho - \Delta E - B\rho$ technique [41, 44]: The beam is guided through two magnets bending in opposite directions. Together with slits, these perform a first selection on the magnetic rigidity of the ions. The acceptance of the FRS is $\pm$ 1.5 % for the momentum of the transmitted beam [45], thus the momentum is rather fixed. At the focal plane behind the two magnets (called S2, c.f. Fig. 3.3), the time of the ions passing through a plastic scintillator is measured, to enable fime-of-flight (ToF) measurements at the FRS and between FRS and experimental setups. A wedge-shaped degrader can be introduced to decelerate the beam. Since the energy loss in scintillator and degrader is proportional to the charge squared of the ions (for a given momentum), the ions are slowed down depending on their charge. The selection is completed by a second set of bending magnets, performing a second selection on the magnetic rigidity, which has changed depending on the charge of the ion due to the energy loss in degrader and scintillator. At the focal plane behind the last two bending magnets (called S8, c.f. Fig. 3.3), another time measurement of the ions passing through a plastic scintillator detector is per-

[3]There are several different kinds of plasma sources used at GSI: Electron Cyclotron Resonance (ECR), Penning Ionization Gauge (PIG), MUlti Cusp Ion Source (MUCIS), Cold or HOt Reflex Discharge Ion Source (CHORDIS), MEtal Vapor Vacuum Arc Ion Source (MEVVA), Vacuum ARc Ion Source (VARIS) and ECRIS CAPRICE. See Refs. [42, 43] for more information.

[4]A standard production target material is beryllium.

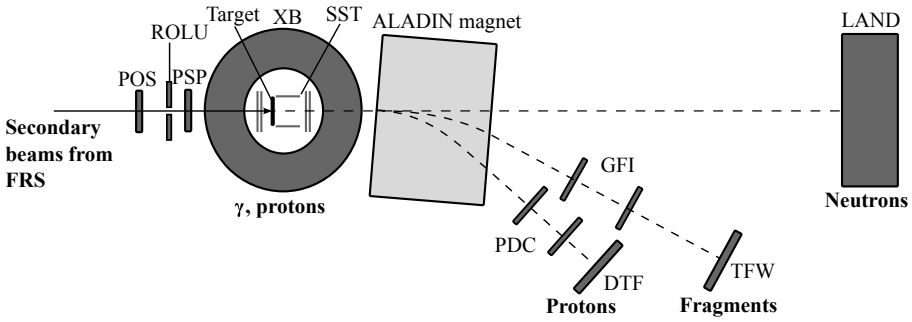

Figure 3.4: Schematic drawing of the S393 experiment at the LAND/R^{3}B setup in top view (not to scale).

formed for the same purpose of ToF measurements as at S2. Thus three ToF measurements are possible S2 – S8, S2 – experiment, and S8 – experiment.
At this stage the creation and selection of the exotic beam is completed and the beam is guided to the experimental setup. Experiments with exotic beams can be performed at the FRS itself, at the storage ring ESR [46] or in the experimental hall. The LAND/R^{3}B setup used for the s393 experiment, leading to papers I, III, IV and V, is located in the experimell hall, in the area called "Cave C".

3.2.1 The LAND/R^{3}B setup

The papers appended to this work, which use the LAND/R^{3}B setup, use it in the s393 version which is sketched in Fig. 3.4.
The incoming beam detectors are POS, ROLU, PSP and two SST detectors. The POS is primarily a timing detector, but can also supply energy-loss and position information. It is a sheet of plastic scintillator with PMT read-out on all four sides. ROLU is an active veto detector, which is solely used to define the size of the beam spot, and is made of four movable plastic scintillators. The PSP (Position Sensitive Pin diode) supplies mainly energy-loss information, but can also be used for position measurements. The anode of the detector has four points for current read-out, one in each corner, and the cathode has one point for that purpose. By the charge collection through a resistive contact, the charge difference between different anode read-out points can be used to reconstruct the position of the impinging particle. The first two SST detectors are placed upstream of the target and are used primarily for position measurement. Each detector is a double-sided silicon strip detector with a pitch size of around 100 μm. They also supply energy-loss information.
Surrounding the target area are more SST detectors, and a NaI(Tl) array,

called Crystal Ball (XB) [47]. Around the target, light particles (n and p) as well as γ-rays need to be detected. This is realized with the NaI array which features a dual read-out [48]: one with a range adjusted to γ-ray detection and one range adjusted to the much larger energy deposited by protons and neutrons. In order to give a better angular resolution and to aid differentiation between protons and neutrons, the SST detectors are grouped as a box around the beam axis just downstream of the target. Due to the relativistic forward focusing, no protons or neutrons are emitted backwards in the laboratory frame of reference. Unfortunately the box detectors did not deliver proper data during the experiment this thesis is concerned with.
Two further SST detectors are positioned downstream of the SST box, in the beam axis to identify the direction of the outgoing fragments and protons in that direction.
All particles emitted inside a 7.5° cone with respect to the beam axis enter the (large-acceptance) dipole magnet ALADIN, where they are deflected according to their magnetic rigidity. Neutrons, not being affected by the magnetic field, continue straight ahead and impinge, after about 12 m flightpath from the target, on the neutron detector LAND [49], which is made of horizontal and vertical bars of sandwiched layers of (passive) iron and plastic scintillators. Using the LANDSHOWER algorithm [50], multiplicity, position and time of the neutrons impinging onto LAND, can be reconstructed.
Fragments and unreacted beam particles are deflected and first detected by two GFI detectors [51]. These are made of vertical scintillating fibres with a cross section area of 1 mm^2, thus giving position information in the bending direction. The detector area is 50 x 50 cm^2. At about 10 m flightpath from the target the fragments are detected in the TFW (180 x 140 cm^2 active area). It is made out of plastic scintillator paddles in both the horizontal and the vertical direction. The primary information supplied by this detector are time and energy-loss. It also supplies a coarse (around 5 cm resolution) position information.
Protons are bent more than the fragments and have significantly smaller energy loss when passing through matter, requiring a separate set of detectors in the forward direction. High-resolution position information in the bending direction is supplied by the PDCs, which are drift chamber detectors. Downstream of those, another ToF wall, the DTF, is located. Similarly to the TFW, it consists of horizontal and vertical plastic scintillator paddles. It supplies time, energy-loss and coarse position information.
More details about the detectors and how they are calibrated can be found in my Licentiate thesis [52].

4. 1p*x*n removal cross sections

In this chapter I will summarize motivation, experiment and analysis of the one-proton removal cross sections measured for neutron-rich boron and carbon isotopes. I will also describe the reaction models used, and give a summary of the comparison.

4.1 Physics motivation

Nuclear physics observables (in combination with the reaction mechanism) need different levels of model-dependent input to be extracted. Angular momentum, which can e.g. be extracted from momentum distributions, is an example an observable depending heavily on the model used. Fragmentation cross sections on the other hand are model-independent, and therefore they are of excellent use to improve model calculations.
But also without comparison to model calculations, cross sections can lead to various discoveries: interaction cross sections measured by Tanihata et al. [15] were used to extract the radii of different Li-isotopes and led to the discovery of halo-nuclei.
Fragmentation cross sections and especially model-calculations predicting these are crucial for planning experiments at accelerator facilities. With the current analysis we want to extend the presently available data on fragmentation reaction cross sections towards the light exotic region and to compare these results with model calculations. Even though fragmentation of such light nuclei is likely not important for yield calculations for accelerator facilities, these cross sections hopefully lead to an improved overall understanding of fragmentation reactions. This in turn benefits accelerator facilities.
With the growing field of using heavy ion beams for cancer treatment, especially beams of ^{12}C, the fragmentation reaction cross sections of the lighter carbon and boron isotopes can contribute to a better knowledge of nuclear reactions which occur during these treatments, and thus to a better under-

standing and calculations of dose-deposition.

4.2 Experiment

The data was collected during a larger experimental campaign with 10 days of beamtime using the LAND/R^{3}B setup at GSI described in Sec. 3.2. The campaign was designed as an overview experiment for light nuclei with Z=3 to Z=9, with a focus on neutron-rich isotopes, but also covering proton-rich isotopes. Its diversity is illustrated by the fact that Papers I, III, IV, V use data from the same experimental campaign, while studying different aspects of light nuclei.
The goal of the experiment is to generally improve the understanding of light exotic nuclei, but it has also a few more concrete goals: to create and study unbound nuclei like ^{16}B, ^{13}Be and ^{25,26}O in (p,2p) reactions on hydrogen. The statistics of the collected data made (p,2p) reaction tagging difficult. The results of ^{25,26}O are published in Paper III and Ref. [52] describes ^{16}B.
Another objective of the experiment is to measure (n,γ) rates for light, neutron-rich nuclei which are relevant for the astrophysical r-process. Results for ^{17}C and ^{19,20}N are published in Paper V and Paper IV, respectively. The third goal is to extract spectroscopic factors using (p,2p) and (p,pn) reactions. Specific focus lies on the oxygen isotopes, but other elements are also to be studied. Several PhD theses have been published with (preliminary) results, see e.g. Refs. [53, 54, 55].
The exotic beams were created by impinging an ^{40}Ar beam with a kinetic energy of 490 MeV/nucleon onto a 4 g/cm^2 beryllium target. The GSI FRS was used to, among the produced isotopes, select ions to be transmitted to the setup. With a total of six different settings of the magnetic rigidity for the secondary beam, the chart of nuclei from stable/proton-rich to the neutron dripline was scanned. The ions had energies in the interval from 390 - 440 MeV/nucleon when entering the setup. Several reaction targets were used during the experiment: carbon, plastic, lead and an empty frame, see Table 4.1 for an overview of thicknesses. The measurements described in this chapter use only data collected with the carbon targets and the empty frame.
The calibration of the setup I have discussed in detail in Ref. [52], thus this is not repeated here, and I describe only the analysis in the following section.

4.3 Analysis

As described previously, in order to calculate cross sections one needs to determine the amount of incoming ions and the amount of ions which underwent the reaction of interest. In the present case this only requires that we identify

Target	thickness $[\mathrm{mg/cm^2}]$
Carbon	$935^{\star\bullet}$
Carbon	$558^{\star}$
Lead	$2145^{\dagger\bullet}$
Plastic	$922^{\bullet}$
empty frame	$-^{\star\bullet\dagger}$

Table 4.1: Overview of the different targets and their thicknesses. Targets marked with $\star$ indicate the targets used in the analysis which is the topic of this chapter. $\bullet$ marks the targets used in Paper III which is described in the next chapter, while † marks the target used in Paper V and Paper IV which are discussed in Ch. 6.

the incoming and the outgoing ions. The following illustrates how this identification is done in Papers I, III, V, IV.
The incoming beam is identified through measurement of time-of-flight and energy-loss together with the magnetic rigidity defined by the fragment separator. The ToF and the well-defined flight path give the velocity. The energy-loss is used to determine the charge of each projectile according to the Bethe-Bloch formula [1]:

$$-\frac{dE}{dx} = \frac{DZ^2 n_e}{\beta^2}\left(\ln\left(\frac{2m_e c_0^2 \beta^2 \gamma^2}{I}\right) - \beta^2 - \frac{\delta(\gamma)}{2}\right) \tag{4.1}$$

with $\frac{dE}{dx}$ being the energy-loss per unit length, Z the charge of the ion, and β the velocity of the ion in units of c, $D = 5.1{\cdot}10^{-25}$ MeV cm^2, n_e the number density of electrons in the material, I the ionization energy of the material, and $\delta(\gamma)$ the dielectric screening correction (depending on Lorentz factor of the ion). From velocity, charge and magnetic rigidity it is then possible to determine the mass of the ion. Fig. 4.1(a) shows the incoming isotopes as identified in this experiment.
For the cross section measurement, using only the energy-loss measurement in the PSP detector leads to too many misidentifications. Therefore, additional energy-loss measurements in the POS and SST2 detectors are used to increase the reliability of the charge measurement, as illustrated in Fig. 4.1(b).
The identification of the outgoing fragments uses the same basic principles. But in contrast to the separation by selective transmission at the FRS, only one magnet is used and different magnetic rigidities are supposed to be transmitted. Another big difference is the material along the beam trajectory: while the beamline to the target holds vacuum, the ALADIN magnet is filled with helium, and behind that the ions travel through air. Together with the material in the detectors, this sums to a significant matter thickness, and thus reaction probability, in comparison to our target. The identification process is therefore

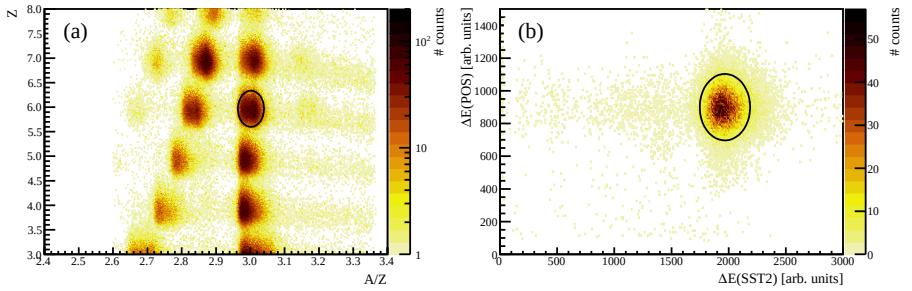

Figure 4.1: Illustration of how the incoming beam is identified. (a) shows the standard method of plotting Z versus A/Z and selecting the incoming isotope by 2σ cuts (determined from a 2D gaussian fit). The charge is determined from the energy loss in the PSP detector. (b) shows an additional means to ensure correct Z-identification, by plotting the energy-loss in two additional detectors (POS and SST2) for a selected isotope (indicated by the ellipse in (a)) and applying an additional 2σ-cut.

more complicated, to ensure that reactions in the setup are excluded as much as possible. The charge identification is thus performed with two energy-loss measurements, one directly behind the target and one at the end of the setup. This is illustrated in Fig. 4.2(a).
To disentangle different masses, the positions of the fragment when traversing the SST and the GFI detectors, together with the magnetic field are used. The mass can be determined from the magnetic rigidity of the fragment. The magnetic rigidity is influenced by the velocity, which in turn is deduced from the ToF and the flight path. The flight path depends on the rigidity. This means there is an interdependence of these quantities and therefore they are determined by an iterative procedure. Since the system is also overdetermined, the iteration is accompanied with a minimization of the χ^2 of actual measurement and calculated path. This is also necessary, since there are substantial effects of (energy and angular) straggling in the setup. This procedure for reconstructing mass, direction and velocity of the fragment behind the target is done using the LAND/R^{3}B TRACKER software [56].
This overall identification and reconstruction procedure is done in approximately the same way for the LAND/R^{3}B papers (Papers I, III, IV, and V).
In order to determine 1p*x*n cross sections, the 0p*x*n and 1p*x*n selections exemplified in Fig. 4.2(a) are tracked and the mass spectra fitted (as shown for the ^{18}C$\rightarrow^{18\text{-}1\text{-}x}$B reaction in Fig. 4.2(b)). With the fits the amount of ions in the unreacted and the 1p*x*n channels are determined from which the cross sections are calculated. For the different cases of unreacted and reacted beam, it

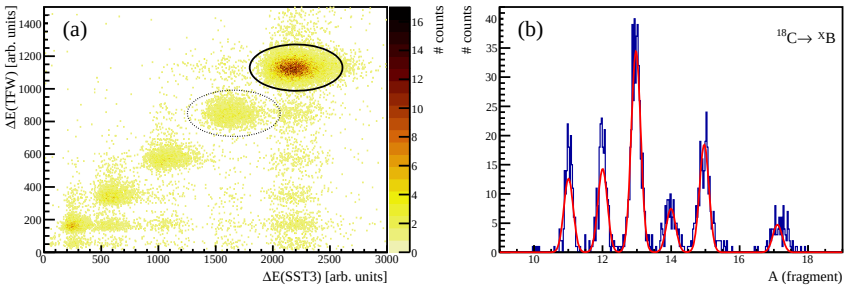

Figure 4.2: Identification of the outgoing beam, using the incoming selection shown in Fig. 4.1. (a) shows energy-loss measurements at the end of the setup in the TFW versus directly behind the target in the SST3. The solid ellipse indicates the selection of events with unchanged charge, and the dotted ellipse indicates the selection of the 1p removal channel. (b) shows the mass spectrum after tracking for the 1p removal channel selected in (a). The red line is a fit of the spectrum.

is necessary to use different hardware trigger[1] conditions to obtain sufficient statistics. For the unreacted beam the "fragment trigger" requiring a signal in POS and in TFW is used. This trigger was unfortunately downscaled[2] strongly, such that the statistics of the reacted beam is not sufficient. Therefore, for selecting the reacted beam, the "XB trigger" is used which requires additionally to the POS and TFW signal also a signal in the XB calorimeter surrounding the target. The trigger efficiency of the "XB trigger" was experimentally determined to be (85.3 $\pm$ 2.5)% of the "fragment trigger". The procedure for determining the trigger efficiency can be found in App. A.

4.4 Reaction models

There exist several reaction models which are, as quite common in nuclear physics, applicable in specific region(s) of the nuclear chart and certain type(s) of reaction(s)[3]. Common types of reaction models for projectile fragmentation are: empirical parametrizations, intranuclear cascade models, and abrasion-

[1] For more information about triggers see Ch. 2.3 of my Licentiate thesis [52].

[2] Downscaling a certain trigger with a factor n means that only every n^{th} event which generates this trigger is stored to disc. If dealing with high beam rates and having triggers which are very likely, but not all of theses events are needed, downscaling is a means to reduce the load on the data acquisition. An example of triggers which are downscaled are triggers corresponding to background events of which a small fraction are needed for monitoring or calibration.

[3] If we do not have a unified model for all nuclei, how should we have a unified model for all reactions?

ablation models. Examples of these model types are EPAX [57], INC [58], and ABRABLA [59] respectively. Paper I compares EPAX3 and ABRABLA07 calculations to the data. Therefore these two are introduced briefly in the following.

4.4.1 EPAX3

EPAX3 is based on an analytic approach, and its main advantage is that it is very fast. EPAX3 uses one formula to calculate the cross section of producing a certain isotope (A,Z) depending on projectile and target isotopes:

$$\sigma(A,Z) = Y_A \sqrt{\frac{R}{\pi}} e^{-R|Z_{prob}-Z|^U} \tag{4.2}$$

The parameters used are the mass yield Y_A, the charge of the isotope with the largest cross section Z_{prob}, and two parameters for the shape: R for the width of the distribution, and U for the (a)symmetry of the distribution.
The parameter U is constant on the proton-rich and the neutron-rich side, but differs depending on the side. All other parameters are fitted to experimental data, and assumed to change smoothly as a function of the fragment, projectile and target mass. A recent introduction is a scale factor for the cross sections on the neutron-rich side, depending on the neutron excess of both projectile and fragment. The code includes a few more additions to resolve a few finer details which can be found in Refs. [60, 61, 62, 63], describing the code and its development.
EPAX3 is limited in the projectile mass region to masses between 40 and 209. It also calculates energy-independent cross sections, which is a valid approximation for sufficiently large beam energies. The lower limit is not clearly defined: reaction cross sections at 140 MeV/nucleon are still well reproduced while those at 64 MeV/nucleon are not, and that kinetic energy is considered to be too low (see Ref. [62]).
EPAX3 is widely used for production rate estimates for secondary beams at facilities around the world. Even though our data is outside the specified mass region for EPAX3, we still compare to it to see how far the use of the model can be extended. Also previous works have compared to EPAX outside of its specified mass region (e.g. Ref. [64]).

4.4.2 ABRABLA07

ABRABLA07 calculates fragmentation and fragmentation-fission cross sections with the ansatz of dividing the reaction into an abrasion and an ablation part. This is justified because of the time scales of the two reaction steps. The abrasion part describes how many nucleons are removed (abraded) in the collision and how much excitation energy is induced. The time scale of this first part

of the reaction is 10^{-21} s. The ablation part describes the de-excitation of the remaining nucleus via light particle evaporation, γ-emission, break-up, and, where appropriate, fission [65]. The time scale of ablation depends on the excitation energy and lies in the range of $(10^{-16} - 10^{-21})$ s for particle emission [59]. ABRABLA07 has no formal restrictions in beam energy or mass of the nucleus. The authors restrict the energy range in which the code is valid to "relativistic beam energies" [59]. It is intended for, and has been tested against, mainly medium-mass to heavy nuclei.
In the abrasion part, the number of removed nucleons is determined from the geometrical overlap of target and projectile nucleus, which depends only on the impact parameter. This is scaled with the total interaction cross section, which is calculated using Karol's approximation [66]. How many abraded nucleons are protons or neutrons is determined assuming that each removed nucleon has a statistical probability to be a proton or a neutron (depending on the A/Z ratio of the projectile), which results in the hypergeometrical distribution. The excitation energy of the pre-fragment is calculated using the average excitation energy. The latter is calculated by assuming a Woods-Saxon potential of -47.4 MeV depth, and a Fermi energy of 7.4 MeV. Assuming that the single-particle level density is proportional to the excitation energy, the model arrives at 13.3 MeV average induced excitation energy per removed nucleon. This procedure assumes that thermalization of the excitation energy does not play a role, which is supported by results from measurements on Ca and Mo [59]. It also neglects any interaction between fireball[4] and spectators, which is not always appropriate, and thus a factor of 2, called excitation energy multiplication factor (f_{EE}), is introduced to cover this effect of final state interactions [67]. The angular momentum of the pre-fragment, which is needed for the ablation process, is calculated in analogy to Goldhaber's [68] calculation of momentum widths.
In the evaporation part, the probabilities for emitting certain particles are obtained from the decay widths, which are calculated according to the Weißkopf-Ewing formalism. The decay widths depend on the excitation energy of the prefragment before and after the collision, the particle type, the kinetic energy of the particle, the level densities of initial and final state, the spin of the particle, the Coulomb barrier (if the particle is charged), and the cross section of the inverse process.
The level densities are calculated based on back-shifted Fermi-gas formula, including corrections for pairing and shell correlations, and folded with enhancement factors for rotational and vibrational contributions, except at very low excitation energies, at which the level densities are calculated using the

[4] At these energies where an abrasion-ablation model is valid, the colliding nuclei can be divided in two parts: the spectators outside of the overlap zone which are assumed not to interact with the other nucleus, and the participants in the overlap zone which are removed from their respective nuclei. The latter form a hot region with energetic nuclei called the fireball.

constant temperature approach. The cross section of the aforementioned inverse process is calculated by neglecting tunnelling through the Coulomb barrier. The tunnelling is then taken into account using a parametrization of its modifications to the decay width. The Coulomb barrier itself is approximated for l=0 particles using an empirical potential. The kinetic energy of the emitted particle is sampled from the Maxwell-Boltzman distribution.
This approach for the ablation step so far completely neglects angular momentum. The distribution of possible angular momenta is calculated and the angular momentum change is picked randomly from that distribution.
Fission and γ emission compete with particle emission (under certain conditions), and their decay widths are calculated in different processes. Especially the calculation of the fission probabilities is rather intricate, and not of interest for light nuclei.
Also γ-emission is of interest mainly for heavier nuclei, and only in the last deexcitation step(s) when the excitation energy $\lesssim S_n$. The decay width for γ-emission is calculated via the giant dipole resonance according to Ref. [69].
At large excitation energies, break-up dominates over fragmentation. In ABRABLA07, if the excitation energy of the pre-fragment exceeds 4.2 MeV per nucleon, the pre-fragment is treated by the break-up routine, and split into several intermediate mass fragments.

4.5 Results and comparison

The results of the cross section measurements are shown in Figs. 4.3 and 4.4 (black squares) together with the calculations performed with ABRABLA07 (red stars, full green circles) and EPAX3 (blue diamonds). The latter is not successful at describing the experimental data. This is not surprising since the nuclei examined here are lighter than the minimal mass specified in EPAX3. Structure effects at the limits of existence are not implemented in EPAX3, and these light nuclei are always close to the drip lines in regard of these calculations.
ABRABLA07 calculations using its standard configuration give the results shown as full green circles. The agreement with the data is unsatisfactory. Unbound isotopes are correctly treated, but otherwise are the cross sections often underestimated and even-odd staggering has the wrong magnitude. Changing the f_{EE} in steps of 0.1 between 0.2 and 2.0, yields an $f_{EE} = 0.6$, which has the best overall fit to the data. This calculation is shown as red stars. The minimization routine to determine the best fit calculation is described in App. B. The best fit calculation is significantly closer to the experimental data than the original configuration of ABRABLA07. The agreement, though not perfect, is surprisingly good for a model that was developed for the description of medium-mass

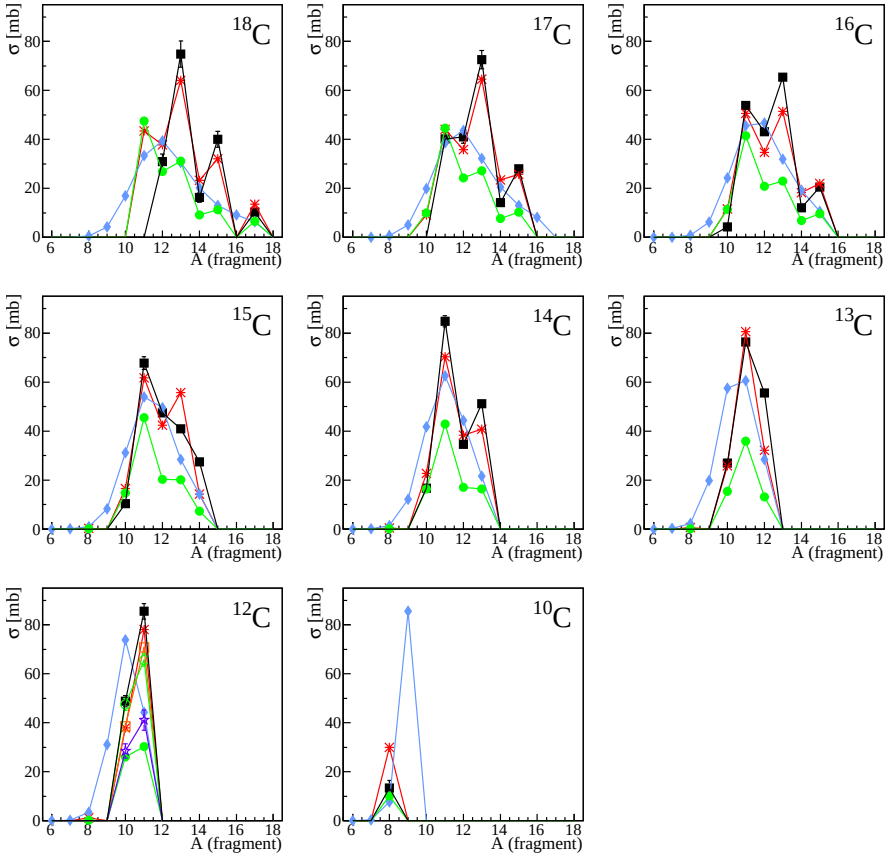

Figure 4.3: Result of the cross section measurement (black full squares) for carbon. The results from the EPAX3 calculation are shown as blue diamonds. The standard ABRABLA07 calculation with $f_{EE} = 2$ is shown as green full circles. The best ABRABLA07 calculation with $f_{EE} = 0.6$ is shown as red stars. Lines are only drawn to guide the eye. Other experimental results are shown for ^{12}C: orange open square - Ref. [70] at 600 MeV/nucleon, green open circle - Ref. [71] at 250 MeV/nucleon, purple bold stars - Ref. [72].

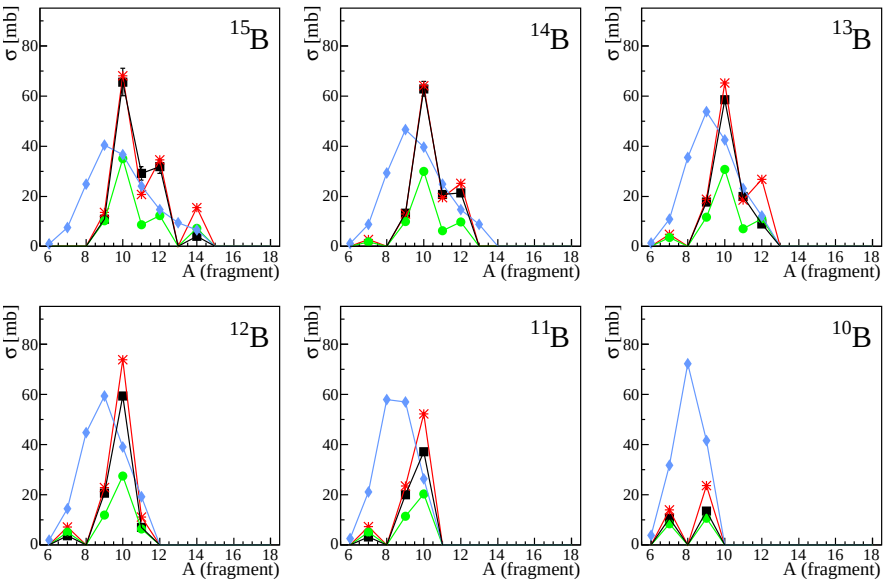

Figure 4.4: Result of the cross section measurement (black full squares) for boron. The results from the EPAX3 calculation are shown as blue diamonds. The standard ABRABLA07 calculation with $f_{EE} = 2$ is shown as green full circles. The best ABRABLA07 calculation with $f_{EE} = 0.6$ is shown as red stars. Lines are only drawn to guide the eye.

to heavy nuclei.
From the argument of fireball-spectator interaction, given in Ref. [67] when introducing an f_{EE} of 2, one could conclude that the interaction should scale with the size of the fireball and the size of the spectator. In order to test this hypothesis, we used the same optimization procedure as above (see App. B), for f_{EE} values between 0.2 and 4, on 1p*x*n cross sections ($x \in [0,5]$) reported in literature, Refs. [70, 73, 74, 75, 76, 77, 78, 79]. For each of the beam isotopes from literature and from this work the best fit f_{EE} was determined. The result is displayed in Fig. 4.5, where one can observe a clear trend of increasing f_{EE} with increasing mass. The results also show a significant spread indicating that the mass of the incoming projectile is not the only parameter influencing the excitation energy. Especially for light isotopes, structure effects may play a bigger role as the induced excitation energy can vary strongly between different removed nucleons. Even peripheral collisions penetrate comparably deep into a small nucleus compared to a heavy one. For small nuclei the approach of an average excitation energy might be too simplistic.
It should be noted that the present results for the heavy nuclei do not contra-

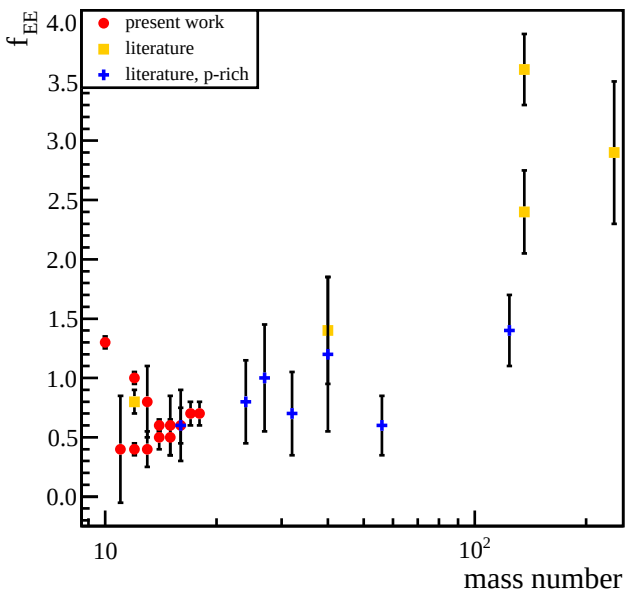

Figure 4.5: Optimal excitation energy multiplication factor versus mass of the beam isotope. Error bars are estimated from the optimization procedure, see App. B for details. Red dots represent the present data and orange squares as well as blue bold crosses represent data from literature. The orange squares show data for beam isotopes with lower neutron-than proton separation energy, the blue crosses indicate the opposite case. The trend of increasing f_{EE} with increasing mass is clear.

dict previous results that yielded an f_{EE} of 2. We restrict here to peripheral collisions (1pxn, $x \in [0,5]$ removal) while the authors of e.g. Ref. [67] analyse a much larger range of created fragments. Instead, the difference between their result and ours indicates that the reaction mechanism (e.g. the impact parameter) also plays a role for the (average) excitation energy, as one would expect.

5. Experiments at the neutron dripline

Light exotic nuclei are expected to provide insights which improve our understanding and description of atomic nuclei (as also discussed in Sec. 1.3). Close to the dripline we find exotic decay modes such as β-delayed particle emission. Usually the β-decay and its subsequent particle emission change the nucleus in the same direction on the nuclear chart, towards stability[1]. That means β^--delayed neutron emission is common on the neutron-rich side, while β^+-delayed proton emission is common on the proton-rich side (β^+-delayed α emission is more common for heavy proton-rich nuclei) [27]. β-delayed deuteron and triton emission are less common, but have been observed. Even the multiparticle βpα decays (βpα), ($\beta\alpha$p), β2p and β2n have been identified [27], and are used to study the structure of the intermediate and final states. Due to the more complicated detection of neutrons than protons (affecting also resolution), proton emitters are better studied than neutron emitters.
But there are also decays which do not bring the daughter significantly closer to the valley of stability, which are energetically allowed in a few neutron- or proton-rich nuclei. Such a decay would e.g. be (β^-p) decay, illustrated in Fig. 5.1. The most favourable case for this decay mode is predicted to be the ^{11}Be nucleus [80, 81]. The branching of (β^-p) decay in this nucleus is estimated to be 10^{-8} [81], with a calculated Q-value of 285.7$\pm$0.2 keV [82]. ^{11}Be is a one-neutron halo nucleus and the (β^-p) decay could proceed as a direct decay of the halo neutron into the continuum [83]. That would offer a new way to study the halo. Sec. 5.1 summarizes the discovery of the (β^-p) decay of ^{11}Be reported in Paper II.
Close to, and at the driplines, we find halo-nuclei and unbound systems just on the other side of the dripline. The latter are not necessarily featureless, but form resonances. The resonances correspond to different discrete energies in the system and are comparable to the level structure in bound nuclei.

[1] This is natural as the separation energy of those nucleons which are in excess in comparison to the stable isobar, is smaller.

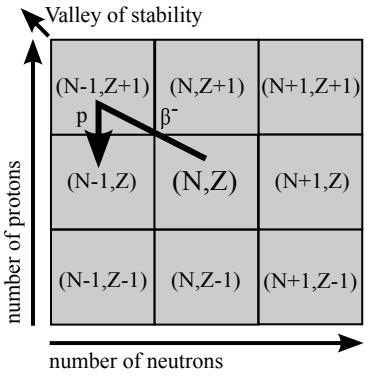

Figure 5.1: Illustration of the path of (β^-p) decay, of a neutron-rich nucleus with N neutrons and Z protons.

By studying the resonances of unbound nuclei, we can learn more about the nuclear interaction close to and in the continuum. Some of the unbound nuclei are subsystems of bound halo nuclei. These are particularly interesting to study, as one can learn more about the corresponding halo nucleus through its subsystem. Lastly, there is no other way to determine the location of the dripline than by measuring which nuclei are bound and which are not.

5.1 Exotic decay near the dripline: (β^- p)

Trying to observe (β^-p) decay, it is natural to attempt the most favourable case, which has been theoretically predicted to be ^{11}Be [80, 81], with a half-life of 13.4 s. This case is particularly interesting, since the decay might involve only the halo neutron, and thus offer a new way to study the halo.
The (theoretical) branching ratio, estimated to be 10^{-8} [81], is experimentally challenging. Due to the small branching ratio and low Q-value of 285.7 $\pm$ 0.2 keV, it is presently not possible to detect the proton and the β-particle in coincidence, allowing for a direct detection of the decay channel. Instead, we detect the decay channel indirectly through its daughter isotope ^{10}Be. This is possible since ^{10}Be is sufficiently long-lived ($1.5 \cdot 10^6$ years [84]). The approach is to collect ^{11}Be by implanting it into a Cu plate, and determine the amount of ions both through recording the implantation current and through the detection of the 2124 keV γ-photon emitted in 34.94 % of the β-decays of ^{11}Be [85]. The amount of ^{10}Be, the daughter nucleus of ^{11}Be(βp), in the sample is then determined by AMS.
A previous attempt [81] could not separate the signal properly from the back-

ground and determined a branching ratio of $(25 \pm 25)\cdot 10^{-6}$, compatible with zero. The VERA facility used for the AMS measurement has now a detection efficiency of $5 \cdot 10^{-4}$, about a factor of 10 better than in the experiment of Ref. [81] in 2001 [86]. Also the yield of ^{11}Be at ISOLDE has been improved.

5.1.1 Possible contamination during sample collection

The Cu samples do not contain ^{10}Be, thus any contamination of the sample would have to be deposited during the collection. That contamination could be caused by isobars of ^{11}Be decaying to ^{10}Be. This would only be ^{11}Li decaying by (βn). Since ^{11}Li is 0.02 mass units heavier than ^{11}Be, separation is not a problem at the HRS. Additionally the yield of ^{11}Li is much lower and can be suppressed by opening the beam gate[2] only 150 ms after proton impact, which is more than 15 times the half-live of ^{11}Li. ^{11}Be has a half-live of 13.81 s, and is thus not affected by the delayed beam gate. The other source of contamination would be molecular ^{10}Be in the form of BeH^-. It is much closer than ^{11}Li to the mass of ^{11}Be, only $3 \cdot 10^{-4}$ mass units away. But since the dissociation energy of this molecule is 3.26 eV and thus much smaller than its ionization energy of 8.22 eV [87], none of these molecules should arrive at the setup. This is confirmed by data from an older experiment [88], which did not use the RILIS source and the RFQ cooler, both of which suppress transmission of molecules.

5.1.2 Results

The amount of deposited ions in the main sample is determined to be $(1.41 \pm 0.19)\cdot 10^{12}$ by the detected 2124 keV γ-rays. From the AMS measurement the amount of ^{10}Be atoms in the sample is determined to $(1.17 \pm 0.05)\cdot 10^{7}$. This yields a branching ratio of $(8.3 \pm 0.9)\cdot 10^{-6}$, which is in agreement with the previous upper limit, but two orders of magnitude larger than the prediction. The branching ratio is clearly larger than zero, and thus one can conclude that β^--delayed proton emission was observed for the first time.
The branching ratio has so far been calculated in one of two ways: either as a decay through a narrow resonance or as a decay directly to the continuum. Both are incompatible with the present decay rate. Interpreting the decay as independent decay of the halo nucleon and a subsequent resonant interaction between proton and core could explain the branching ratio. However, so far

[2] Ions are not always accelerated and guided towards the separators, but only during a certain period, the beam gate, after proton impact on the production target. This has two reasons: the HV cannot be stabilized during proton impact, and thus the kinetic energy would be ill-defined, and a certain time after proton impact radioactive species have decayed and the remaining stable ones are not of interest.

no resonance in ^{11}B, which would fit this decay mechanism, is known.
Presently the analysis of another measurement with the same setup is ongoing.

5.2 Dripline crossing: neutron-unbound nuclei

In this section the results on the investigated unbound nuclei will be presented. The measurements on ^{25,26}O and ^{16}B were performed with the LAND/R^{3}B setup, in the same experiment as described in Ch. 4. The identification of the outgoing fragment is performed as described in that chapter. For reconstruction of the unbound system, the unbound nucleon(s), in this case neutron(s), need to be observed. Neutrons are detected in the LAND detector, and their ToF(s), multiplicity and position(s) are extracted using the LANDSHOWER algorithm. The energy of the unbound system is then reconstructed as the relative energy, described in Sec. 2.1.
Initially these systems were intended to be studied by (p,2p) reaction tagging, identifying quasi-free scattering when producing the unbound systems and thus minimizing the effect of the production mechanism on the unbound nuclei. Unfortunately a shortened beam-time[3] and reprioritization, as well as lower yields than expected, led to significantly lower statistics, for the ^{16}B case by a factor of 10 [52]. Therefore, the use of this more restrictive reaction selection is not possible. For the oxygen case, all available targets are used. In the analysis for boron only the data collected with carbon and plastic targets are used.

5.2.1 The unbound oxygen isotopes

The reconstructed relative energy of the ^{25}O system (reconstructed from ^{24}O + n) is shown in Fig. 5.2. The fit of the data with a Breit-Wigner function with $l = 2$, reproduces the data well. The width and position of the resonance is given in Table 5.1, which summarizes the presently available data on the ground states of ^{25,26}O.
The case for ^{26}O is a little bit more intricate. The relative energy of the ^{24}O$+n+n$ system is shown in Fig. 5.3, using two different bin sizes. In the upper panel two Breit-Wigner shaped resonances are fitted without background. The lower panel features the same Breit-Wigner functions with the same type of non-resonant background as in the ^{25}O case. The result of these fits is that the lower-lying resonance is located at 25 $\pm$ 25 keV and the higher-energy resonance at around 4 MeV. Fitting the non-resonant background alone to the data in 1 MeV wide bins (blue, dotted line), clearly shows that this does not reproduce the data.

[3] Caused by problems in the accelerator.

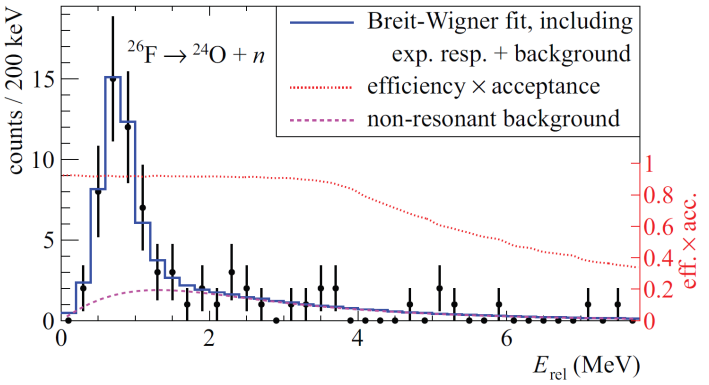

Figure 5.2: Relative energy of the ^{25}O system. The red dotted curve indicates the efficiency and acceptance of the setup. The magenta dashed curve shows the modelled non-resonant background. Both are included in the blue solid curve which shows a Breit-Wigner fit with $l = 2$ to the data. Error bars are purely statistical. Figure from Paper III.

As can be seen from the efficiency and acceptance curve in the top panel, the setup has limited acceptance for very low relative energies. This is caused by the need to separate the two neutrons impinging on the same detector, which is not possible if they hit the detector close to each other. In that case only one neutron will be reconstructed and the two neutrons will be mistaken for one. These events thus show up in the $^{27}F \rightarrow ^{24}O + 1\ n$ channel, which has been included in the fit shown in the top panel of Fig. 5.3.
With the given statistics, and since the resonance is at such a low energy where the acceptance changes strongly, there is no possibility to extract the width (and thus lifetime) of the ground state resonance from the fit of the spectrum. Instead, one can use the reconstructed fragment mass spectrum to identify if

$E_r(^{26}O)$	$\tau(^{26}O)$	$E_r(^{25}O)$	$\Gamma(^{25}O)$	Ref.	Year
18(5)	-	749(10)	88(6)	[13]	2016
-	4.5 ± 3.4 ps	-	-	[89]	2013
25(25)	≤ 5.7 ns	725^{+54}_{-29}	20^{+60}_{-20}	Paper III	2013
150^{+50}_{-150}	-	-	-	[90]	2012
-	-	770^{+20}_{-10}	172(30)	[91]	2008

Table 5.1: Summary of the experimental results on the ground state resonance energy and width in keV for ^{26}O and ^{25}O. Energies are measured in keV from the ground state energy of ^{24}O.

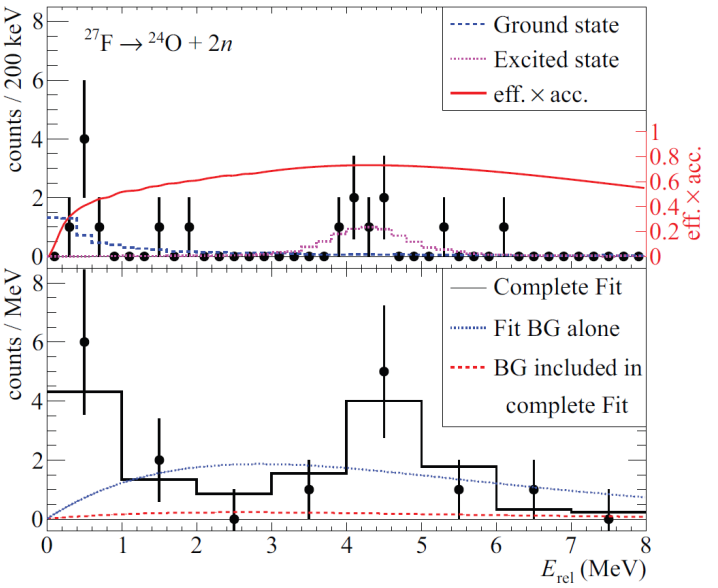

Figure 5.3: Spectrum of the relative energy of the ^{26}O system. The data in both panels is identical but analysed with different bin sizes, 200 keV in the top and 1 MeV in the bottom panel. The top panel presents the efficiency and acceptance curve of the setup for 2n events (red solid). Two states are fitted at 25 keV (blue dashes) and 4 MeV respectively (magenta dotted). The bottom panel shows a fit if only the background function is used (blue dotted) and a fit (black solid) using both resonances and the non-resonant background (dotted red). Figure from Paper III.

there are any events that might originate from a surviving ^{26}O. If the ^{26}O resonance lives longer than it takes to travel through the setup to the centre of the magnet, it will be reconstructed at masses above 24. This flight time is 11.8 ns and one event could be identified, though it cannot be excluded that it belongs to background. On the basis of this one event one can determine the upper limit of the lifetime of this state, which at 95% confidence corresponds to 5.7 ns or a width of at least $1.2 \cdot 10^{-10}$ keV.

The data, except for the width of the ^{25}O ground state, agrees within error bars with previously measured data, see Table 5.1. Very recently the data from an experiment at RIBF have been published [13] having more statistics and thus much smaller statistical uncertainties. The data agree within error bars with the data presented here. Anyhow none of the other experiments were able to extract a width of the ^{26}O ground state, so the lower limit provided in

Ref.	year	g.s. [keV]	τ / Γ (g.s.)	other
[93]	1974			proof unbound
[94]	1985			proof unbound
[95]	1995	40(60)		
[96]	1996		191 ps	
[97]	2000	40(60)	$\leq$ 100 keV	excited state: 2.32(7) MeV
[98]	2009	85(15)		transverse mom., rel. energy
[99]	2010	60(20)	$\ll$ 100 keV	rel. energy

Table 5.2: Summary of previous experimental work on ^{16}B.

Paper III is the only information at present. Ref. [89] published shortly after Paper III derived a more restrictive lifetime of (4.5 $\pm$ 3.4) ps from the velocity shift between neutrons and fragment. A more restrictive limit on the width (or lifetime) of the state would be necessary to determine the angular momentum quantum number (or numbers in case of mixed states) of the resonance. It cannot be determined even from the restrictive energy interval provided by Ref. [13] and the limit from Paper III which still allow for a s-, p- and d-type resonance when comparing to theoretical calculations from Ref. [92]. The data from Ref. [89] basically excludes the s-state.

5.2.2 Unbound ^{16}B

The lightest unbound boron isotope, ^{16}B has been proven to be unbound by Bowman *et al.* [93]. Since then several experiments on ^{16}B have been performed, see Table 5.2. Shell model calculations [100] and microscopic cluster calculations [101] have been performed, both predicting several low-lying excited states. We intended to produce ^{16}B with the exclusive (p,2p) reaction mechanism and to record γ-rays from the system for a first time.
The reconstructed relative energy for the ^{16}B system is shown in Fig. 5.4. The data is not corrected for acceptance, but as shown in the previous section (see Fig. 5.2), the acceptance is constant in the displayed energy interval. One can see that the contribution of the random background is negligible (red data points). The figure shows that there are no strong differences between carbon and plastic target data. The difference (in blue) is due to the hydrogen in the plastic target. Unfortunately the statistics is not sufficient to perform a deeper analysis with the contribution from only the hydrogen in the target. Initially it was intended to study the hydrogen target[4] data with an additional selection using the signature of protons stemming from a quasi-free (p,2p) reaction. Since this cuts the amount of statistics by roughly a factor of 3 [52],

[4]The hydrogen target would be reconstructed, as above, from the plastic target with its carbon contribution subtracted.

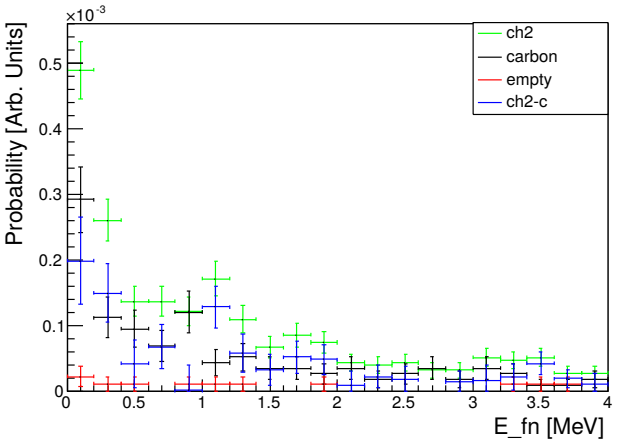

Figure 5.4: Relative energy of the ^{16}B system produced in collisions with different targets, scaled to the same amount of incoming ions. Green shows the data collected with the plastic target, and black data collected with the carbon target. Data collected with the plastic target with its carbon contribution subtracted is plotted in blue. Data points in red are collected with an empty target frame.

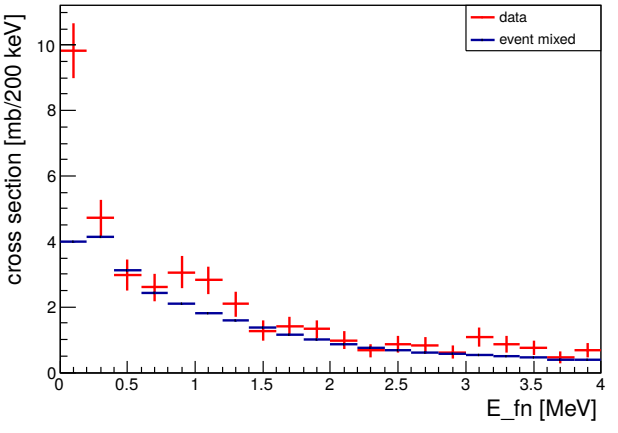

Figure 5.5: Relative energy of the ^{16}B system from carbon and plastic target (red). The non-resonant background (blue) was determined by event-mixing (see text). Two resonances are visible above background.

this analysis is not meaningful.
Instead the statistics from the carbon and plastic targets are added, which gives the relative energy spectrum shown in Fig. 5.5 (red). The statistical error bars are still significant. To avoid a fit of the non-resonant background (shown in blue), the latter is determined from event-mixing. The event-mixing works as follows: from the ^{16}B dataset neutrons and fragments from different events are paired up randomly, and the relative energy of that system is computed. The data and the non-resonant background indicate that the ground state resonance of ^{16}B is located below 200 keV, and that there is a resonance at around 1 MeV. The ground state resonance agrees with previous data in Refs. [98, 99], producing ^{16}B by proton removal at lower energies. However none of them have observed an excited state. Kalpakchieva *et. al* [97], used transfer reactions and their ground state is in agreement with the later works. They have found an unconfirmed higher lying resonance at 2.32(7) MeV, but none at 1 MeV.
The experiment recorded γ-rays coincident with ^{16}B for the first time, but no clear evidence of γ-emission could be found.

6. Neutron capture cross sections of light neutron-rich nuclei

One of the key questions in nuclear astrophysics is where and how isotopes heavier than Fe are synthesized. The p-process[1] and s-process (slow neutron capture), which are rather well understood, account for the creation of about half of the heavy elements [102, 103], but especially the abundances above A=100 cannot be explained without another process [104]. So the other half of the elements heavier than iron is believed to be created in the r-process (rapid neutron capture process), in an environment of high temperature ($\sim$ 1 GK) and large neutron density (10^{20} - 10^{28} neutrons/cm^3) [105]. Candidate sites are core-collapse supernovae, neutron-star mergers, (accretion discs of) neutron-star black-hole mergers and γ-ray bursts.
The r-process creates elements by adding neutrons to the nuclei at the site, the seed nuclei, in a series of (n,γ) reactions and thus proceeds through the very neutron-rich region. Usually at some point equilibrium is established between (n,γ) and (γ,n) reactions, and the rate of the creation of one isotope will thus be larger than the subsequent ones. This isotope is called waiting point. β^- decay from mainly that waiting point isotope (but also the other ones, depending on half-lives and capture rates) feeds higher-Z elements. Thus the path (more appropriately the web) of the r-process and the final abundance of the created isotopes depends on masses which determine neutron capture and Coulomb dissociation[2] cross sections, β-decay rates, (βn)-decay rates, as well as the pressure, temperature, neutron density, and the time-development of these during the event. It also depends on the seed nuclei, which in turn depend on the conditions listed above (and on the history of the object). There are different models calculating the isotopic yields adapted to different astrophysical

[1] This was earlier thought to be a process of proton-capture, but nowadays is believed to proceed via Coulomb dissociation (γ,p) (γ, α) reactions.

[2] Another name of this process is photo-dissociation.

scenarios. The nuclear physics input, so far, mainly relies on theoretical estimates of masses, decay- and reaction rates, as there is very little experimental data available this far from stability. These theoretical rates and masses have large uncertainties since the nuclei are far from stability, and thus it is difficult to identify the astrophysical site of the event. Measuring the properties of neutron-rich nuclei is therefore very important to advance the understanding of the r-process.
Since there are hundreds of isotopes involved in the r-process, it is reasonable to determine which reaction rates or masses have the largest influence on the final abundances. This is done by systematically changing reaction rates and masses in the calculation frameworks and by comparing the change in final abundances, in sensitivity studies. For more details see, e.g., recent reviews [106, 102].

6.1 Motivation

Most r-process model calculations focus on neutron-rich nuclei in the heavy region, but only very few consider light nuclei away from stability, because seed nuclei are expected to be heavy ($A \geq 70$). Extending the reaction network for calculations to the neutron dripline for $Z \leq 10$ nuclei, Terasawa *et al.* [107] show that these light exotic nuclei can play an important role as seed nuclei in the r-process for models with high neutron density and rapidly dropping temperature, as might be found in neutrino-driven wind[3] core-collapse supernovae, prompt explosions of supernovae or binary neutron star mergers. A subsequent sensitivity study identifies neutron capture rates on ^{17}C as important input data also because the theoretical uncertainty is large (a factor of 10) [108].
Through the inverse process of Coulomb dissociation, exploiting the principle of detailed balance, we have measured neutron capture rates of ^{17}C and ^{20,21}N.

6.2 Experiment

The data was collected in the s393 experiment as described in Sec. 3.2. In order to determine the neutron capture cross section, we measure the Coulomb dissociation cross section. Apart from reconstructing the fragment mass and four-vector, as described in Ch. 4, it is necessary to detect the outgoing γ-rays and their energy and to detect emitted neutrons and to reconstruct their four-momenta. The latter is extracted with the help of the LANDSHOWER

[3]There are several models of how a core-collapse supernova evolves. One model assumes that huge amounts of neutrinos are generated in the gravitational shock. These travel outwards and heat the outer layers. This can lead to all nuclei dissociating into p, n, and α particles, thus removing heavy seed nuclei and generating light ones.

Isotope	state	σ [mb]
^{17}C	g.s.	32 ± 13
	1^{st} exc.	40 ± 8
	2^{nd} exc.	43 ± 6
	total	115 ± 11
^{20}N	g.s.	15 ± 16
	1^{st} exc.	36 ± 6
	total	90 ± 12
^{21}N	g.s.	31 ± 16
	1^{st} & 2^{nd} exc.	47 ± 8
	total	75 ± 13

Table 6.1: Summary of the Coulomb dissociation cross sections, measured in Paper IV and Paper V. The errors are purely statistical.

algorithm. The detected γ-energies were added in clusters of neighbouring crystals (by the add-back routine, see e.g. [52]) and Doppler corrected[4]. The γ-energies were then used to gate on different states which are populated in the dissociation reaction. Paper V used the energies of the different clusters, while Paper IV used the XB detector as a calorimeter and uses the full sum of γ-energies instead.
Gating on the different excited states, cross sections for Coulomb dissociation to ground, first and second excited states as well as the total Coulomb dissociation cross section were determined.

6.3 Results

For dissociation to ^{17}C, cross sections to ground, first and second excited state could be derived. For dissociation to ^{19}N, cross sections to ground and first excited state as well as to all excited states (up to 5 MeV) were determined. Due to the experimental resolution it is not possible to separate the first and second excited state of ^{20}N from the γ-spectrum and thus the dissociation cross sections to ground, sum of first and second excited state, and all excited states (up to 5 MeV) were determined. The cross sections are summarized in Table 6.1.

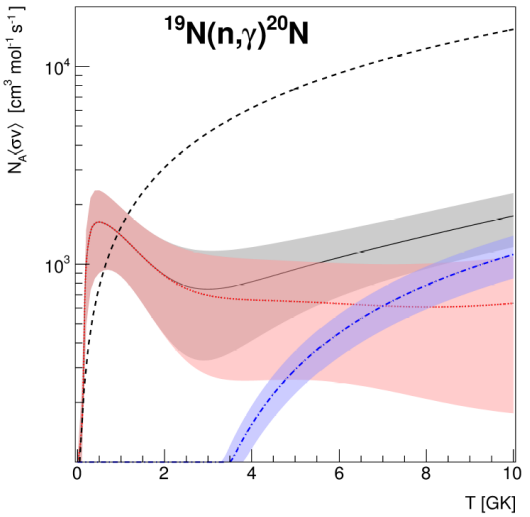

Figure 6.1: Experimental stellar reaction rate for neutron capture on ^{19}N (solid line). The contributions of ground state (dotted) and first excited state (dash-dotted) are indicated separately. The shaded area indicates the statistical uncertainty. Calculations by Ref. [109] are shown for comparison. Figure from Paper IV.

6.4 Impact on r-process calculations

Using the virtual photon theory and the principle of detailed balance it is possible to calculate the neutron capture cross section from the Coulomb dissociation cross section [110]:

$$\sigma_{n,\gamma} = \frac{2(2I_{\text{in}}+1)}{(2I_{\text{out}}+1)(2I_{\text{n}}+1)} \frac{k_\gamma^2}{k_{\text{c.m.}}^2} \frac{d\sigma_{\text{CD}}}{dE^*} \frac{1}{n_{\text{E1}}(E^*)} E^* \tag{6.1}$$

with σ_{CD} denoting the Coulomb dissociation cross section, E^* the excitation energy and n_{E1} the number of virtual photons. I stands for the spin of the neutron, the incoming and the outgoing ion of the Coulomb dissociation reaction respectively, and k the momenta of the photon and the neutron-fragment system, respectively.
In the context of astrophysics, the neutron capture cross section needs to be folded with the distribution of the velocity of the neutrons to calculate reaction rates (depending on temperature). As an example of the results, Fig. 6.1 displays the stellar neutron capture rate of ^{19}N. These capture rates can be

[4]Low energies in single crystals are background-suppressed.

used as input to r-process calculations.
Running network calculations simulating the conditions of a neutrino-driven-wind supernova scenario to determine the impact of the neutron capture rates of nitrogen, the reference calculations used the rates of the sensitivity study quoted above [108] and the neutron capture rate of ^{19}N from Ref. [109], which is also shown in Fig. 6.1. Using the experimental reaction rates for nitrogen leads to a decrease of the abundance of fluorine by 10 % in comparison to the reference calculations. The abundances of heavy elements are not affected.
In order to determine the effect of the neutron capture rate of ^{17}C, calculations modelling a neutrino-driven wind supernova and a neutron star merger were performed. The same reaction rates as used by Sasaqui *et al.* in their sensitivity study [108], which identified ^{17}C as important, were used. Also here the reaction rate of ^{17}C, though differing from the reference by about a factor of two, did not affect the abundances of heavy elements ($\leq$ 0.1 %). Some elements below mass 20 were affected.
Concluding, the measured reaction rates did not affect the final abundances of heavy elements in the astrophysical conditions used here. They should however be included in future calculations, as they have proven relevant in other studies [107, 108]. To identify the astrophysical site(s) of the r-process, more experimental neutron capture cross sections and β-decay rates are needed to decrease the uncertainties.

7. Discussion and Conclusions

Paper I points out that the ability of ABRABLA07 to describe fragmentation reactions depends on the average induced excitation energy per nucleon. We observe a mass dependence of the induced average excitation energy per nucleon for the 1pxn ($x \leq 5$) reaction channels. This result, obtained with a restricted set of reaction channels, disagrees with the average excitation energy (per nucleon) derived from the full set of measured cross sections for gold producing iridium and platinum (Ref. [67]), indicating that the reaction channel also influences the induced average excitation energy (per nucleon). This dependence on the reaction channel can also be seen in other heavy nuclei, e.g. in xenon, as shown in Fig. 7.1. In this figure the difficulty of describing all measured 1pxn channels with the same average excitation energy per nucleon (parametrized by the f_{EE}) is clearly visible. Since the impact parameter (which we cannot measure) determines how likely certain reactions channels are, the selection of the latter is also a rough selection in impact parameter. The impact parameter might thus be one important parameter determining how much average excitation energy *per nucleon* is induced[1], as the contribution of final state interactions seems to be coupled to it. Ref. [111] has found that the average induced excitation energy depends on isospin. Together these studies show that ABRABLA07 would benefit from a more realistic description of the excitation energy depending on mass, isospin and reaction channel or impact parameter.

One might argue that a theory that can describe all isotopes, the goal of nuclear physics research, is not furthered by a model like ABRABLA07. But we do not only need a theory which can describe atomic nuclei from first principles, which will most likely rely on massive calculations and huge matrices, we also need models which enhance our intuitive understanding of nuclear processes. ABRABLA07 breaks the description down into smaller parts and ap-

[1] Here the emphasis is on the *average per nucleon*. The impact parameter also governs how many nucleons are removed and through that how much excitation energy enters the system, but that the average per nucleon depends on the impact parameter is not part of the model (so far).

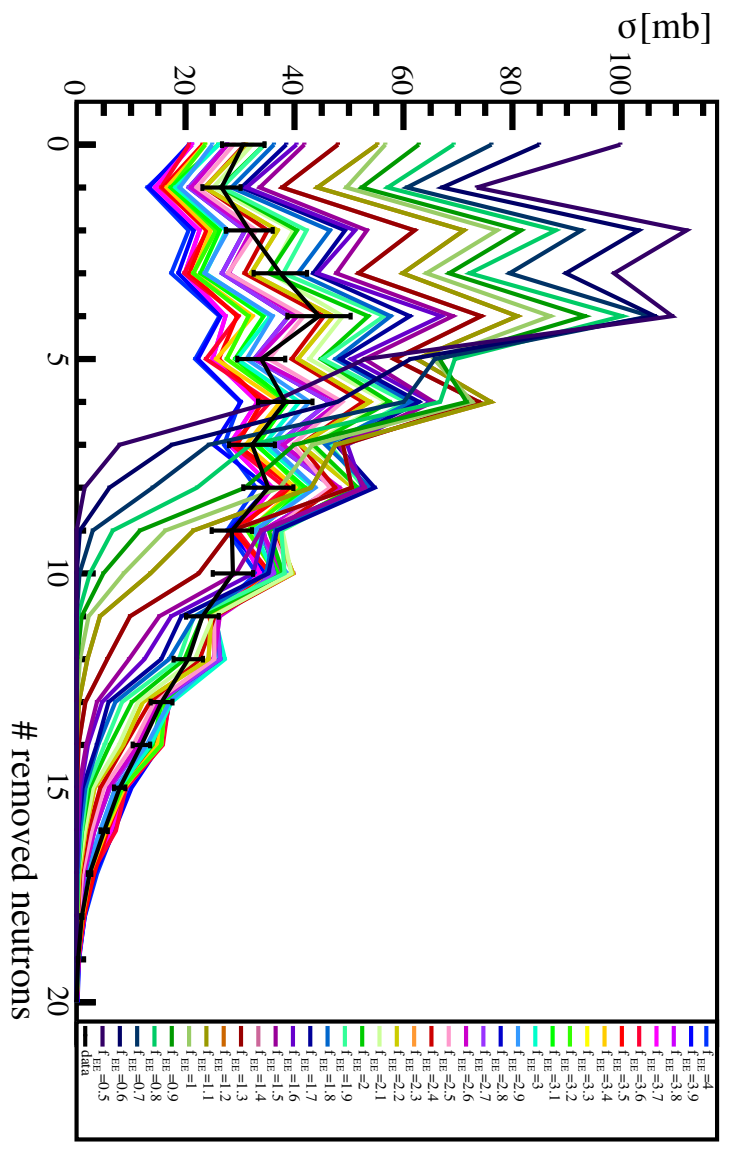

Figure 7.1: 1pxn cross section from ^{136}Xe on (black stars); data taken from Ref. [76]. Abrabla calculations with different f_{EE} (colour coded) are compared to the data. One can see three different groups of reaction channels in the comparison and that these yield different f_{EE}, if regarded separately.

proximates the physics in these, e.g.: it calculates the total interaction cross sections with Karol's approximation.Independent of this approximation, the impact parameter is used to calculate how many nucleons are removed. By using approximations based on physics arguments in the different subparts (as well divided with the help of physics arguments), ABRABLA07 improves our understanding and has shown to be surprisingly successful. Thus augmenting the description of the induced excitation energy in ABRABLA07 based on (intuitive) physics arguments will not only improve this model but also further our understanding in general.
The unbound ^{25,26}O measured in Paper III confirm the oxygen anomaly and agree with previous and more recent data. The need of proper description of three-nucleon interactions is emphasized as ^{26}O cannot be correctly described otherwise. The question of ^{26}O decaying by 2n emission is, based on the results in Paper III, rather likely as the ground state energy of ^{25}O is larger than that of ^{26}O. Kondo *et al.* [13] assume in their analysis that the ground state of ^{26}O decays by 2n emission, while they show that the first excited state they found stems from sequential decay through ^{25}O. This paper shows also what probably would have been possible if the experiment that delivered data for Paper III and on ^{16}B would not have suffered from beam-time shortening and re-prioritization. With enough statistics we could have performed an analysis similar to the one by Kondo *et al.* already in 2013. The importance of proper planning, preparation and execution of nuclear physics experiments is illustrated by the insufficient statistics on ^{16}B, which does not enable us to improve on previous data. Nuclear physics experiments are challenging and expensive, and thus it is seldom possible to rerun an experiment[2] which means that everything has to work out or buffer time needs to be planned for.
Paper II finds (β^-p)-decay for the first time. The results point at an independent decay of the halo-neutron, which would be the first proof of this kind of decay. If the decay proceeds in this manner we will be able to learn more about the halo via decay spectroscopy. This would, however, require a high beam rate due to the small branching ratio, which would generate a large background from normal β-decay. Additionally is the Q-value rather low, yielding a small kinetic energy of the proton and with that difficulties in the detection. For spectroscopy, significant improvements of the detection system are necessary to allow for a direct detection of the emitted proton.
Papers IV and V study astrophysical relevant neutron capture processes which improve our understanding of the r-process. The results did not show a large impact on the calculations performed in the papers, although that was expected from a sensitivity study [108] for the ^{17}C(n,γ)^{18}C rate. Sensitivity studies are an important tool to give indications of which reaction channels are important, but are not without challenges. Since the sensitivity studies themselves rely on input parameters depending of the (so far unsettled) astro-

[2] It is not completely impossible. The smaller the experiment, the higher the chances of a rerun.

physical site of the r-process, this induces a large uncertainty in the results of the sensitivity studies: the reactions having a large impact in one scenario do not need to have the same impact in another scenario. Thus, until the site of the r-process is identified, it is rather difficult to judge the importance of these reaction rates.

The nuclei and observables studied in this work are different and related at the same time. The division in the previous chapters emphasizes the differences between the different groups, but all the studies aim at a common goal: to improve the description of atomic nuclei. They try to further our understanding of the nuclear interaction in specific areas of nuclear physics, may it be decay or astrophysics. This improved understanding (hopefully) spreads from its specific corner and will reach the other realms of nuclear physics, since they all belong together.
Concluding, the papers presented in this work all contribute small pieces to the puzzle which is nuclear physics. At present we take small steps, but generally research consists of a lot of small steps and a few bigger ones, breakthroughs, once in a while. These breakthroughs are typically not seen before they happen, the next one might be just ahead of us.
Nuclear physics does not only contribute to a better understanding of how nuclei work, it exports knowledge to other fields. The methodology developments and technical progress in radiation detection we drive to enable our advanced measurements, benefit monitoring detectors and sensors. Two well-known examples of nuclear physics inspired ideas in medicine are PET scanners and ion beam therapy.
Additionally, the field of big data recently discovered event-based data, a basic approach which has been used for a long time in nuclear physics. I think this field could learn a lot about data treatment from the experience we have in the field of nuclear physics. With the new facilities producing larger amounts of data and theoretical approaches already heavily relying on computations, nuclear physics might soon be driving certain computational aspects, too.

8. Outlook

To continue the research in Paper I I would like to analyse the heavier isotopes in the same dataset. Even more importantly one can extract cross sections on other reaction channels like 0p*x*n and 2p*x*n removal. Reaction channels from removal of more than two protons might be possible to analyse especially for the heavier isotopes. While the 0p1n and 0p2n removal channels are not problematic as far as detector acceptance is concerned, one needs to look at the trigger patterns and their trigger efficiency for these channels. For the removal of more protons, simulations of the acceptance are necessary. A proper tool would e.g. be GGLAND, as a recent bachelor project [112] shows. The simulations need to give a proper quantification of the acceptance for different reaction channels. This might also enable an extension to more than 5 neutrons in the 1p*x*n removal channel. It would also be interesting to use the data on heavier isotopes from literature and to see how the dependence of the excitation energy (per nucleon) depends on the selected reaction channels (and thus impact parameter) and how this can be understood.
Concerning the oxygen isotopes, Paper III has already been superseded by Ref. [13]. To improve on these data, simultaneous collection of γ-rays would be interesting. Performing an experiment with conditions ideal for (p,2p) reactions, it would be interesting to see if such a "minimally-invasive" production mechanism has an impact on the observed relative energy. To determine the width of the ground state of ^{26}O is a challenge. Experimental resolution is finite and will probably not increase sufficiently for a direct measurement in the near future. Thus further lifetime measurements with more statistics and a reliable analysis method are, in my opinion, the biggest chance of determining a width of the ground state. At the future R^{3}B setup at FAIR, higher beam intensities and a simultaneous detection of γ-rays as well as (p,2p) reaction tagging can be achieved. Another interesting aspect is ^{28}O, and the question whether it is more or less bound than ^{26}O. Based on classical shell closures it should be more bound than ^{26}O, but the shell closure at ^{24}O indicates the breakdown of the classical shell structure for neutron-rich oxygen isotopes. An experiment recently performed at RIBF (with participation from the Chalmers group), might provide an answer to that question.

Analysis of another experiment as in Paper II is ongoing, to verify the result. Spectroscopy of the proton would be very interesting as already mentioned above. Unfortunately is the, still unexpectedly large, branching ratio, of (8.3 $\pm$ 0.9)$\cdot 10^{-6}$ very small. I thus do not expect that a spectroscopy experiment will be possible in the near future.
Concerning the r-process and experimental contributions, (n,γ)-rates, beta-decay rates, and (α,γ)-rates are important to measure. Close collaboration with model developments and sensitivity studies are necessary to identify the most crucial reactions in this vast amount of unmeasured reactions, for which theoretical predictions are not reliable. Also in this case the R^3B setup at FAIR and similar setups at RIBF and FRIB will be well suited to measure (n,γ) reaction cross sections of light and heavy nuclei. Due to the high beam energies of FAIR, the cross sections will be most favourable there.

More generally the next-generation nuclear physics facilities are already operational or on the doorstep: RIBF started delivering beam in 2008, FAIR and FRIB are under construction right now. The new and bigger facilities allow for larger and more complex experiments. The consequences of that need to be understood. Already now the time from proposal to experiment to published data exceeds the time-span of the PhD education at the larger setups. All these steps are, however, part of research and need to be experienced during the PhD education. We also need to be aware that more complicated detector systems need a higher degree of knowledge in order to allow for method development. This means that it might not be possible to combine method development and physics analysis in one PhD project, while both are important parts of nuclear physics and should be honoured. The higher level of knowledge needed from detector- (or reconstruction-) experts has also general consequences: the high fluctuation rate of these experts, usually in the post-doc phase, leads to loss of knowledge, which needs to be avoided. I can see two ways to improve the situation: less fluctuation, by creating longer term positions for the detector experts, or a higher degree of documentation and communication.
The higher complexity of the experiments naturally leads to larger collaborations, as many people are needed to run the entire setup, because almost each detector needs experts. Thus the experiment collaborations grow from about 20 people to several hundreds. While a team of 20 people is easily organized and communicated with, several hundreds are different. We need to professionalize the handling of collaborations and especially the communication inside of them. I think it would be healthy to learn from the particle physics community, which has taken this step already quite some time ago, with their biggest experiments involving several thousand contributors nowadays.
A third consequence of the increased complexity is more intricate data handling and analysis. Nuclear physics is not the only field which treats huge amounts of complicated data, apart from the exchange with particle phys-

ics, we might be able to benefit from knowledge in astronomy and big data and vice-versa. Also these developments should therefore be communicated (i.e. published) such that they are accessible to other fields, which they are too seldom at present.

Bibliography

[1] K. A. Olive and Particle Data Group. “Review of Particle Physics”. In: *Chin. Phys. C* 38.9 (2014), p. 090001. URL: http://stacks.iop.org/1674-1137/38/i=9/a=090001.

[2] B. R. Martin. *Nuclear and Particle Physics*. 2nd ed. John Wiley and Sons Ltd, 2011.

[3] *National Nuclear Data Center*. Brookhaven National Laboratory. URL: http://www.nndc.bnl.gov/.

[4] M. G. Mayer. “Nuclear Configurations in the Spin-Orbit Coupling Model. I. Empirical Evidence”. In: *Phys. Rev.* 78.1 (Apr. 1950), pp. 16–21. DOI: 10.1103/PhysRev.78.16.

[5] R. F. Casten. *Nuclear Structure from a Simple Perspective*. Ed. by P. E. Hodgson. 2nd ed. Oxford Science Publications, 2000.

[6] C. Forssén, G. Hagen, M. Hjorth-Jensen, W. Nazarewicz and J. Rotureau. “Living on the edge of stability, the limits of the nuclear landscape”. In: *Phys. Scr.* T152 (2013), p. 014022. URL: http://stacks.iop.org/1402-4896/2013/i=T152/a=014022.

[7] Y. Blumenfeld, T. Nilsson and P. V. Duppen. “Facilities and methods for radioactive ion beam production”. In: *Phys. Scr.* T152 (2013), p. 14023. URL: http://stacks.iop.org/1402-4896/2013/i=T152/a=014023.

[8] P. Van Duppen. “Isotope Separation On Line and Post Acceleration”. In: *The Euroschool Lectures on Physics with Exotic Beams*. Ed. by J. Al-Khalili and E. Roeckl. Vol. II. Lecture Notes in Physics. Springer Berlin Heidelberg, 2006. Chap. 2, pp. 37–77. DOI: 10.1007/b11743651.

[9] B. A. Marsh. “Resonance ionization laser ion sources for on-line isotope separators”. In: *Rev. Sc. Instr.* 85.2, 02B923 (2014). DOI: 10.1063/1.4858015.

[10] H. L. Ravn. “Experiments with intense secondary beams of radioactive ions”. In: *Phys. Rep.* 54.3 (1979), pp. 201–259. DOI: http://dx.doi.org/10.1016/0370-1573(79)90045-0.

[11] L. Penescu, J. Lettry, T. Stora, R. Catherall and G. Cata-Danil. "Arc Discharge Ion Source Development at CERN ISOLDE". In: *Univ. Politeh. Buchar. Sci. Bull., A* 72.2 (2010), pp. 121–132. URL: http://cds.cern.ch/record/1359345.

[12] D. J. Morrissey and B. M. Sherrill. "In-Flight Separation of Projectile Fragments". In: *The Euroschool Lectures on Physics with Exotic Beams*. Ed. by J. S. Al-Khalili and E. Roeckl. Vol. I. Lecture Notes in Physics. Springer Berlin Heidelberg, 2004. Chap. 4, pp. 113–135. DOI: 10.1007/b98790.

[13] Y. Kondo, T. Nakamura, R. Tanaka, R. Minakata, S. Ogoshi, N. A. Orr, N. L. Achouri, T. Aumann, H. Baba, F. Delaunay, P. Doornenbal, N. Fukuda, J. Gibelin, J. W. Hwang, N. Inabe, T. Isobe, D. Kameda, D. Kanno, S. Kim, N. Kobayashi, T. Kobayashi, T. Kubo, S. Leblond, J. Lee, F. M. Marqués, T. Motobayashi, D. Murai, T. Murakami, K. Muto, T. Nakashima, N. Nakatsuka, A. Navin, S. Nishi, H. Otsu, H. Sato, Y. Satou, Y. Shimizu, H. Suzuki, K. Takahashi, H. Takeda, S. Takeuchi, Y. Togano, A. G. Tuff, M. Vandebrouck and K. Yoneda. "Nucleus ^{26}O: A Barely Unbound System beyond the Drip Line". In: *Phys. Rev. Lett.* 116 (10 Mar. 2016), p. 102503. DOI: 10.1103/PhysRevLett.116.102503.

[14] T. Baumann, A. M. Amthor, D. Bazin, B. A. Brown, C. M. Folden III, A. Gade, T. N. Ginter, M. Hausmann, M. Matos, D. J. Morrissey, M. Portillo, A. Schiller, B. M. Sherrill, A. Stolz, O. B. Tarasov and M. Thoennessen. "Discovery of Mg-40 and Al-42 suggests neutron drip-line slant towards heavier isotopes". In: *Nature* 449.7165 (Oct. 2007), 1022–1024. DOI: 10.1038/nature06213.

[15] I. Tanihata, H. Hamagaki, O. Hashimoto, Y. Shida, N. Yoshikawa, K. Sugimoto, O. Yamakawa, T. Kobayashi and N. Takahashi. "Measurements of Interaction Cross Sections and Nuclear Radii in the Light p-Shell Region". In: *Phys. Rev. Lett.* 55 (24 Dec. 1985), pp. 2676–2679. DOI: 10.1103/PhysRevLett.55.2676.

[16] P. G. Hansen and B. Jonson. "The Neutron Halo of Extremely Neutron-Rich Nuclei". In: *Eur. Phys. Lett.* 4.4 (1987), p. 409. URL: http://stacks.iop.org/0295-5075/4/i=4/a=005.

[17] K. Riisager. "Halos and related structures". In: *Phys. Scr.* T152 (2013), p. 014001. URL: http://stacks.iop.org/1402-4896/2013/i=T152/a=014001.

[18] H. Simon. "Halo nuclei, stepping stones across the drip-lines". In: *Phys. Scr.* T152 (2013), p. 014024. URL: http://stacks.iop.org/1402-4896/2013/i=T152/a=014024.

[19] R. Kanungo. “A new view of nuclear shells”. In: *Phys. Scr.* T152 (2013), p. 014002. URL: http://stacks.iop.org/1402-4896/2013/i=T152/a=014002.

[20] R. Kanungo, C. Nociforo, A. Prochazka, T. Aumann, D. Boutin, D. Cortina-Gil, B. Davids, M. Diakaki, F. Farinon, H. Geissel, R. Gernhäuser, J. Gerl, R. Janik, B. Jonson, B. Kindler, R. Knöbel, R. Krücken, M. Lantz, H. Lenske, Y. Litvinov, B. Lommel, K. Mahata, P. Maierbeck, A. Musumarra, T. Nilsson, T. Otsuka, C. Perro, C. Scheidenberger, B. Sitar, P. Strmen, B. Sun, I. Szarka, I. Tanihata, Y. Utsuno, H. Weick and M. Winkler. “One-Neutron Removal Measurement Reveals ^{24}O as a New Doubly Magic Nucleus”. In: *Phys. Rev. Lett.* 102 (15 Apr. 2009), p. 152501. DOI: 10.1103/PhysRevLett.102.152501.

[21] H. Sakurai, S. M. Lukyanov, M. Notani, N. Aoi, D. Beaumel, N. Fukuda, M. Hirai, E. Ideguchi, N. Imai, M. Ishihara, H. Iwasaki, T. Kubo, K. Kusaka, H. Kumagai, T. Nakamura, H. Ogawa, Y. E. Penionzhkevich, T. Teranishi, Y. X. Watanabe, K. Yoneda and A. Yoshida. “Evidence for particle stability of ^{31}F and particle instability of ^{25}N and ^{28}O”. In: *Phys. Lett. B* 448.3 - 4 (1999), pp. 180–184. DOI: 10.1016/S0370-2693(99)00015-5.

[22] E. K. Warburton, J. A. Becker and B. A. Brown. “Mass systematics for A = 29 - 44 nuclei: The deformed $A \sim$32 region”. In: *Phys. Rev. C* 41 (3 Mar. 1990), pp. 1147–1166. DOI: 10.1103/PhysRevC.41.1147.

[23] C. Thibault, R. Klapisch, C. Rigaud, A. M. Poskanzer, R. Prieels, L. Lessard and W. Reisdorf. “Direct measurement of the masses of ^{11}Li and $^{26\text{-}32}$Na with an on-line mass spectrometer”. In: *Phys. Rev. C* 12 (2 Aug. 1975), pp. 644–657. DOI: 10.1103/PhysRevC.12.644.

[24] X. Campi, H. Flocard, A. Kerman and S. Koonin. “Shape transition in the neutron rich sodium isotopes”. In: *Nucl. Phys. A* 251.2 (1975), pp. 193–205. DOI: 10.1016/0375-9474(75)90065-2.

[25] K. Heyde and J. L. Wood. “Shape coexistence in atomic nuclei”. In: *Rev. Mod. Phys.* 83 (4 Nov. 2011), pp. 1467–1521. DOI: 10.1103/RevModPhys.83.1467.

[26] A. Gade and S. N. Liddick. “Shape coexistence in neutron-rich nuclei”. In: *J. Phys. G* 43.2 (2016), p. 024001. URL: http://stacks.iop.org/0954-3899/43/i=2/a=024001.

[27] M. J. G. Borge. “Beta-delayed particle emission”. In: *Phys. Scr.* T152 (2013), p. 014013. URL: http://stacks.iop.org/1402-4896/2013/i=T152/a=014013.

[28] A. M. Lane and R. G. Thomas. “R-Matrix Theory of Nuclear Reactions”. In: *Rev. Mod. Phys.* 30 (2 Apr. 1958), pp. 257–353. DOI: 10.1103/RevModPhys.30.257.

[29] T. Aumann, C. A. Bertulani and J. Ryckebusch. “Quasifree $(p,2p)$ and (p,pn) reactions with unstable nuclei”. In: *Phys. Rev. C* 88 (6 Dec. 2013), p. 064610. DOI: 10.1103/PhysRevC.88.064610.

[30] C. A. Bertulani and P. G. Hansen. “Momentum distributions in stripping reactions of radioactive projectiles at intermediate energies”. In: *Phys. Rev. C* 70 (3 Sept. 2004), p. 034609. DOI: 10.1103/PhysRevC.70.034609.

[31] Y. Aksyutina, T. Aumann, K. Boretzky, M. G. Borge, C. Caesar, A. Chatillon, L. V. Chulkov, D. Cortina-Gil, U. Datta Pramanik, H. Emling, H. O. U. Fynbo, H. Geissel, G. Ickert, H. T. Johansson, B. Jonson, R. Kulessa, C. Langer, T. LeBleis, K. Mahata, G. Münzenberg, T. Nilsson, G. Nyman, R. Palit, S. Paschalis, W. Prokopowicz, R. Reifarth, D. Rossi, A. Richter, K. Riisager, G. Schrieder, H. Simon, K. Sümmerer, O. Tengblad, H. Weick and M. V. Zhukov. “Momentum profile analysis in one-neutron knockout from Borromean nuclei”. In: *Phys. Lett.* B718.4–5 (2013), pp. 1309–1313. DOI: 10.1016/j.physletb.2012.12.028.

[32] M. Pfützner, M. Karny, L. V. Grigorenko and K. Riisager. “Radioactive decays at limits of nuclear stability”. In: *Rev. Mod. Phys.* 84 (2 Apr. 2012), pp. 567–619. DOI: 10.1103/RevModPhys.84.567.

[33] W.-M. Yao, C. Amsler, D. Asner, R. Barnett, J. Beringer, P. R. Burchat, C. D. Carone, C. Caso, O. Dahl, G. D’Ambrosio, A. DeGouvea, M. Doser, S. Eidelman, J. L. Feng, T. Gherghetta, M. Goodman, C. Grab, D. E. Groom, A. Gurtu, K. Hagiwara, K. G. Hayes, J. J. Hernández-Rey, K. Hikasa, H. Jawahery, C. Kolda, Y. Kwon, M. L. Mangano, A. V. Manohar, A. Masoni, R. Miquel, K. Mönig, H. Murayama, K. Nakamura, S. Navas, K. A. Olive, L. Pape, C. Patrignani, A. Piepke, G. Punzi, G. Raffelt, J. G. Smith, M. Tanabashi, J. Terning, N. A. Törnqvist, T. G. Trippe, P. Vogel, T. Watari, C. G. Wohl, R. L. Workman, P. A. Zyla, B. Armstrong, G. Harper, V. S. Lugovsky, P. Schaffner, M. Artuso, K. S. Babu, H. R. Band, E. Barberio, M. Battaglia, H. Bichsel, O. Biebel, P. Bloch, E. Blucher, R. N. Cahn, D. Casper, A. Cattai, A. Ceccucci, D. Chakraborty, R. S. Chivukula, G. Cowan, T. Damour, T. DeGrand, K. Desler, M. A. Dobbs, M. Drees, A. Edwards, D. A. Edwards, V. D. Elvira, J. Erler, V. V. Ezhela, W. Fetscher, B. D. Fields, B. Foster, D. Froidevaux, T. K. Gaisser, L. Garren, H.-J. Gerber, G. Gerbier, L. Gibbons, F. J. Gilman, G. F. Giudice, A. V. Gritsan, M. Grünewald, H. E. Haber, C. Hagmann, I. Hinchliffe, A. Höcker, P. Igo-Kemenes, J. Jackson, K. F. Johnson, D. Karlen, B. Kayser, D. Kirkby, S. R. Klein, K. Kleinknecht, I. G. Knowles, R. V. Kowalewski, P. Kreitz, B. Krusche, Y. V. Kuyanov, O. Lahav, P. Langacker, A. Liddle, Z. Ligeti, T. M. Liss, L. Littenberg, L. Liu, K. S. Lugovsky, S. B. Lugovsky, T. Mannel, D. M. Manley, W. J. Marciano, A. D. Martin, D. Milstead, M. Narain, P. Nason, Y. Nir, J. A. Peacock,

S. A. Prell, A. Quadt, S. Raby, B. N. Ratcliff, E. A. Razuvaev, B. Renk, P. Richardson, S. Roesler, G. Rolandi, M. T. Ronan, L. J. Rosenberg, C. T. Sachrajda, S. Sarkar, M. Schmitt, O. Schneider, D. Scott, T. Sjöstrand, G. F. Smoot, P. Sokolsky, S. Spanier, H. Spieler, A. Stahl, T. Stanev, R. E. Streitmatter, T. Sumiyoshi, N. P. Tkachenko, G. H. Trilling, G. Valencia, K. van Bibber, M. G. Vincter, D. R. Ward, B. R. Webber, J. D. Wells, M. Whalley, L. Wolfenstein, J. Womersley, C. L. Woody, A. Yamamoto, O. V. Zenin, J. Zhang and R.-Y. Zhu. "Review of Particle Physics". In: *J. Phys. G* 33 (2006), pp. 1+. URL: http://pdg.lbl.gov.

[34] T. Aumann. "Uncovering the properties of exotic nuclei via reactions with relativistic radioactive beams". In: *Rutherford Centennial Conference on Nuclear Physics*. Vol. 381. Journal of Physics Conference Series. 2012. DOI: 10.1088/1742-6596/381/1/012008.

[35] *ISOLDE Logos, Layouts and Templates*. Accessed: 2016.05.13. URL: http://isolde.web.cern.ch/isolde-logos-layouts-and-templates#.

[36] E. Kugler. "The ISOLDE facility". In: *Hyperfine Interact.* 129.1 (2000), pp. 23–42. DOI: 10.1023/A:1012603025802.

[37] H. Frånberg, P. Delahaye, J. Billowes, K. Blaum, R. Catherall, F. Duval, O. Gianfrancesco, T. Giles, A. Jokinen, M. Lindroos, D. Lunney, E. Mane and I. Podadera. "Off-line commissioning of the ISOLDE cooler". In: *Nucl. Instrum. Methods B* 266.19 - 20 (2008). DOI: 10.1016/j.nimb.2008.05.097.

[38] M. J. G. Borge. "Highlights of the ISOLDE Facility and the HIE-ISOLDE Project". In: *Acta Phys. Pol. B* 47.3 (Mar. 2016), 591–605. DOI: 10.5506/APhysPolB.47.591.

[39] W. Kutschera, P. Collon, H. Friedmann, R. Golser, P. Hille, A. Priller, W. Rom, P. Steier, S. Tagesen, A. Wallner, E. Wild and G. Winkler. "VERA: A new AMS facility in Vienna". In: *Nucl. Instrum. Methods B* 123.1–4 (1997), pp. 47–50. DOI: 10.1016/S0168-583X(96)00782-3.

[40] V. N. Fedoseyev, G. Huber, U. Köster, J. Lettry, V. I. Mishin, H. Ravn and V. Sebastian. "The ISOLDE laser ion source for exotic nuclei". In: *Hyperfine Interact.* 127.1 (2000), pp. 409–416. DOI: 10.1023/A:1012609515865.

[41] H. Geissel, P. Armbruster, K. H. Behr, A. Brünle, K. Burkard, M. Chen, H. Folger, B. Franczak, H. Keller, O. Klepper, B. Langenbeck, F. Nickel, E. Pfeng, M. Pfützner, E. Roeckl, K. Rykaczewski, I. Schall, D. Schardt, C. Scheidenberger, K.-H. Schmidt, A. Schröter, T. Schwab, K. Sümmerer, M. Weber, G. Münzenberg, T. Brohm, H.-G. Clerc, M. Fauerbach, J.-J. Gaimard, A. Grewe, E. Hanelt, B. Knödler, M. Steiner, B. Voss, J. Weckenmann, C. Ziegler, A. Magel, H. Wollnik, J. P. Dufour, Y. Fujita,

D. J. Vieira and B. Sherrill. “The GSI projectile fragment separator (FRS): a versatile magnetic system for relativistic heavy ions”. In: *Nucl. Instrum. Methods B* 70.1 (1992), pp. 286–297. DOI: 10.1016/0168-583X(92)95944-M.

[42] R. Hollinger, K. Tinschert, A. Adonin, M. Brühl, B. Gutermuth, F. Heymach, R. Lang, J. Mäder, F. Maimone, K. Ochs, J. Pfister, J. Rossbach, P. Schäffer, S. Schäffer, M. Stork, C. Vierheller, A. Wesp and S. Zulauf. “Ion Source Operation at the GSI Accelerator Facility”. In: *GSI scientific report 2011* (2012). URL: https://www.gsi.de/fileadmin/Ion_Sources/Scientific_reports/2011/Ion_source_Operation_-_2.pdf.

[43] *FAIR@GSI: Linac and Operation: Ion Sources*. Accessed May 17th 2016. URL: https://www.gsi.de/en/work/fairgsi/linac_and_operations/ion_sources/sources/ion_sources.htm?nr=/proc/self/env.

[44] B. Voss, T. Brohm, H.-G. Clerc, A. Grewe, E. Hanelt, A. Heinz, M. de Jong, A. Junghans, W. Morawek, C. Röhl, S. Steinhäuser, C. Ziegler, K.-H. Schmidt, K.-H. Behr, H. Geissel, G. Münzenberg, F. Nickel, C. Scheidenberger, K. Sümmerer, A. Magel and M. Pfützner. “The scintillation-detector equipment of the GSI projectile-fragment separator”. In: *Nucl. Instrum. Methods A* 364.1 (1995), pp. 150–158. DOI: 10.1016/0168-9002(95)00294-4.

[45] J. Benlliure, J. Pereira-Conca and K.-H. Schmidt. “New approach to determine the angular transmission in zero-degree magnetic spectrometers”. In: *Nucl. Instrum. Methods A* 478.3 (2002), pp. 493–505. DOI: 10.1016/S0168-9002(01)00893-2.

[46] B. Franzke. “The heavy ion storage and cooler ring project ESR at GSI”. In: *Nucl. Instrum. Methods B* 24 (1987), pp. 18–25. DOI: 10.1016/0168-583X(87)90583-0.

[47] V. Metag, R. D. Fischer, W. Kühn, R. Mühlhans, R. Novotny, D. Habs, U. v. Helmholt, H. W. Heyng, R. Kroth, D. Pelte, D. Schwalm, W. Hennerici, H. J. Hennrich, G. Himmerle, E. Jaeschke, R. Repnow, W. Wahl, E. Adelberger, A. Lazzarini, R. S. Simon, R. Albrecht and B. Kolb. “Physics with 4π γ-Detectors”. In: *Nucl. Phys.* A409 (1983), pp. 331–342.

[48] F. Wamers. “Quasi-free Knockout Reactions with the Proton-dripline Nucleus ^{17}Ne at Relativistic Beam Energies”. PhD thesis. TU Darmstadt, 2011.

[49] T. Blaich et al. “A Large area detector for high-energy neutrons”. In: *Nucl. Instrum. Methods* A314 (1992), pp. 136–154. DOI: 10.1016/0168-9002(92)90507-Z.

[50] J. G. Keller and E. F. Moore. “Shower Recognition and Particle Identification in LAND”. In: *GSI scientific report 1991* 1 (1992), p. 39.

[51] K. Mahata, H. T. Johansson, S. Paschalis, H. Simon and T. Aumann. "Position reconstruction in large-area scintillating fibre detectors". In: *Nucl. Instrum. Methods* A608 (2009), pp. 331–335. DOI: 10.1016/j.nima.2009.07.012.

[52] R. Thies. *Across the drip-line and back: examining ^{16}B*. Licentiate thesis - Department of Fundamental Physics, Chalmers University of Technology, No: 112. 2014. URL: https://publications.lib.chalmers.se/publication/193345-across-the-drip-line-and-back-examining-16b.

[53] P. Díaz Fernández. "An investigation into quasi-free scattering of light neutron-rich nuclei around N=14". PhD thesis. Universidade de Santiago de Compostela, 2013.

[54] M. A. Najafi. "Quasi-free proton and neutron knockout reactions in ^{20}O". PhD thesis. University of Groningen, 2013.

[55] M. Holl. "Quasi-Free Scattering from Relativistic Neutron-deficient Carbon Isotopes". PhD thesis. TU Darmstadt, 2014.

[56] R. Plag. *Documentation on the LAND/R^3B tracker*. http://ralfplag.de/tracker. GSI. 2015.

[57] K. Sümmerer and H. Weick (C translation). *[C source code] EPAX Version 3 : An Empirical Parametrization of Projectile-Fragmentation Cross Sections, 17.01.2013*. https://www-alt.gsi.de/documents/DOC-2012-May-55.html. Jan. 2013.

[58] Y. Yariv and Z. Fraenkel. "Intranuclear cascade calculation of high energy heavy ion collisions: Effect of interactions between cascade particles". In: *Phys. Rev. C* 24 (2 Aug. 1981), pp. 488–494. DOI: 10.1103/PhysRevC.24.488.

[59] J.-J. Gaimard and K.-H. Schmidt. "A reexamination of the abrasion-ablation model for the description of the nuclear fragmentation reaction". In: *Nucl. Phys.* A531.3–4 (1991), pp. 709–745. DOI: 10.1016/0375-9474(91)90748-U.

[60] K. Sümmerer, W. Brüchle, D. J. Morrissey, M. Schädel, B. Szweryn and Y. Weifan. "Target fragmentation of Au and Th by 2.6 GeV protons". In: *Phys. Rev. C* 42 (6 Dec. 1990), pp. 2546–2561. DOI: 10.1103/PhysRevC.42.2546.

[61] K. Sümmerer and B. Blank. "Modified empirical parametrization of fragmentation cross sections". In: *Phys. Rev. C* 61 (3 Feb. 2000). DOI: 10.1103/PhysRevC.61.034607.

[62] K. Sümmerer. "Improved empirical parametrization of fragmentation cross sections". In: *Phys. Rev. C* 86 (1 July 2012), p. 014601. DOI: 10.1103/PhysRevC.86.014601.

[63] K. Sümmerer. “Erratum: Improved empirical parametrization of fragmentation cross sections [Phys. Rev. C **86** , 014601 (2012)]”. In: *Phys. Rev. C* 87 (3 Mar. 2013), 039903(E). DOI: 10.1103/PhysRevC.87.039903.

[64] A. Leistenschneider, T. Aumann, K. Boretzky, L. F. Canto, B. V. Carlson, D. Cortina, U. Datta Pramanik, Th. W. Elze, H. Emling, H. Geissel, A. Grünschloss, K. Helariutta, M. Hellström, M. S. Hussein, S. Ilievski, K. L. Jones, J. V. Kratz, R. Kulessa, Le Hong Khiem, E. Lubkiewicz, G. Münzenberg, R. Palit, P. Reiter, C. Scheidenberger, K.-H. Schmidt, H. Simon, K. Sümmerer, E. Wajda and W. Walús. “Fragmentation of unstable neutron-rich oxygen beams”. In: *Phys. Rev. C* 65 (6 May 2002), p. 064607. DOI: 10.1103/PhysRevC.65.064607.

[65] A. Kelic, M. V. Ricciardi and K.-H. Schmidt. “ABLA07 - towards a complete description of the decay channels of a nuclear system from spontaneous fission to multifragmentation”. In: *Joint ICTP-IAEA Advanced Workshop on Model Codes for Spallation Reactions Trieste, Italy, February 4-8, 2008*. 2009. URL: http://inspirehep.net/record/823871/files/arXiv:0906.4193.pdf.

[66] P. J. Karol. “Nucleus-nucleus reaction cross sections at high energies: Soft-spheres model”. In: *Phys. Rev. C* 11 (4 Apr. 1975), 1203–1209. DOI: 10.1103/PhysRevC.11.1203.

[67] K.-H. Schmidt, T. Brohm, H.-G. Clerc, M. Dornik, M. Fauerbach, H. Geissel, A. Grewe, E. Hanelt, A. Junghans, A. Magel, W. Morawek, G. Münzenberg, F. Nickel, M. Pfützner, C. Scheidenberger, K. Sümmerer, D. Vieira, B. Voss and C. Ziegler. “Distribution of Ir and Pt isotopes produced as fragments of 1 A GeV ^{197}Au projectiles: a thermometer for peripheral nuclear collisions”. In: *Phys. Lett.* B 300.4 (1993), pp. 313–316. DOI: 10.1016/0370-2693(93)91338-N.

[68] A. S. Goldhaber. “Statistical models of fragmentation processes”. In: *Phys. Lett. B* 53.4 (1974), pp. 306–308. DOI: 10.1016/0370-2693(74)90388-8.

[69] A. V. Ignatyuk. In: *Proceedings on of the Conference Bologna 2000: Structure of the Nucleus at the Dawn of the Century*. Ed. by G. C. Bonsignori, M. Bruno, A. Ventura and D. Vretenar. World Scientific, 2001. DOI: 10.1142/9789812810922_0053.

[70] W. R. Webber, J. C. Kish and D. A. Schrier. “Individual isotopic fragmentation cross sections of relativistic nuclei in hydrogen, helium, and carbon targets”. In: *Phys. Rev. C* 41 (2 Feb. 1990), pp. 547–565. DOI: 10.1103/PhysRevC.41.547.

[71] J. M. Kidd, P. J. Lindstrom, H. J. Crawford and G. Woods. “Fragmentation of carbon ions at 250 MeV/nucleon”. In: *Phys. Rev. C* 37 (6 June 1988), pp. 2613–2623. DOI: 10.1103/PhysRevC.37.2613.

[72] T. Ogawa, T. Sato, S. Hashimoto, D. Satoh, S. Tsuda and K. Niita. “Energy-dependent fragmentation cross sections of relativistic ^{12}C”. In: *Phys. Rev. C* 92 (2 Aug. 2015), p. 024614. DOI: 10.1103/PhysRevC.92.024614.

[73] D. Pérez-Loureiro et al. “Production of neutron-rich nuclei in fragmentation reactions of ^{132}Sn projectiles at relativistic energies”. In: *Phys. Lett.* B703 (2011), pp. 552–556. DOI: 10.1016/j.physletb.2011.08.037.

[74] T. Kurtukian-Nieto, J. Benlliure, K.-H. Schmidt, L. Audouin, F. Becker, B. Blank, E. Casarejos, F. Farget, M. Fernández-Ordóñez, J. Giovinazzo, D. Henzlova, B. Jurado, J. Pereira and O. Yordanov. “Production cross sections of heavy neutron-rich nuclei approaching the nucleosynthesis r -process path around $A = 195$”. In: *Phys. Rev. C* 89 (2 Feb. 2014), p. 024616. DOI: 10.1103/PhysRevC.89.024616.

[75] A. R. Junghans, M. de Jong, H.-G. Clerc, A. V. Ignatyuk, G. A. Kudyaev and K.-H. Schmidt. “Projectile-fragment yields as a probe for the collective enhancement in the nuclear level density”. In: *Nucl. Phys.* A629.3–4 (1998), pp. 635–655. DOI: 10.1016/S0375-9474(98)00658-7.

[76] D. Henzlova, K.-H. Schmidt, M. V. Ricciardi, A. Kelić, V. Henzl, P. Napolitani, L. Audouin, J. Benlliure, A. Boudard, E. Casarejos, J. E. Ducret, T. Enqvist, A. Heinz, A. Junghans, B. Jurado, A. Krása, T. Kurtukian, S. Leray, M. F. Ordóñez, J. Pereira, R. Pleskac, F. Rejmund, C. Schmitt, C. Stéphan, L. Tassan-Got, C. Villagrasa, C. Volant, A. Wagner and O. Yordanov. “Experimental investigation of the residues produced in the Xe-136+Pb and Xe-124+Pb fragmentation reactions at 1-A-GeV”. In: *Phys. Rev. C* 78 (2008), p. 044616. DOI: 10.1103/PhysRevC.78.044616.

[77] J. Benlliure, M. Fernández-Ordóñez, L. Audouin, A. Boudard, E. Casarejos, J. E. Ducret, T. Enqvist, A. Heinz, D. Henzlova, V. Henzl, A. Kelic, S. Leray, P. Napolitani, J. Pereira, F. Rejmund, M. V. Ricciardi, K.-H. Schmidt, C. Schmitt, C. Stéphan, L. Tassan-Got, C. Volant, C. Villagrasa and O. Yordanov. “Production of medium-mass neutron-rich nuclei in reactions induced by Xe-136 projectiles at 1-A-GeV on a beryllium target”. In: *Phys. Rev. C* 78 (2008), p. 054605. DOI: 10.1103/PhysRevC.78.054605.

[78] B. Fernández-Domínguez, R. C. Lemmon, B. Blank, M. Chartier, D. Cortina-Gil, J. L. Durell, H. Geissel, J. Gerl, S. Mandal, F. Rejmund and K. Sümmerer. "Production cross-sections from neutron-deficient ^{92}Mo at 500*A* MeV". In: *Eur. Phys. J.* A25.2 (2005), pp. 193–198. DOI: 10.1140/epja/i2005-10104-5.

[79] B. Fernández-Domínguez, R. C. Lemmon, B. Blank, M. Chartier, D. Cortina-Gil, J. L. Durell, H. Geissel, J. Gerl, S. Mandal, F. Rejmund and K. Sümmerer. "Erratum: Production cross-sections from neutron-deficient ^{92}Mo at 500*A* MeV". In: *Eur. Phys. J.* A25.3 (2005), pp. 473–474. DOI: 10.1140/epja/i2005-10159-2.

[80] D. Baye and E. M. Tursunov. "β delayed emission of a proton by a one-neutron halo nucleus". In: *Phys. Lett. B* 696.5 (2011), pp. 464–467. DOI: 10.1016/j.physletb.2010.12.069.

[81] M. J. G. Borge, L. M. Fraile, H. O. U. Fynbo, B. Jonson, O. S. Kirsebom, T. Nilsson, G. Nyman, G. Possnert, K. Riisager and O. Tengblad. "Rare p decays in light nuclei". In: *J. Phys. G* 40.3 (2013), p. 035109. URL: http://stacks.iop.org/0954-3899/40/i=3/a=035109.

[82] M. Wang, G. Audi, A. H. Wapstra, F. G. Kondev, M. MacCormick, X. Xu and B. Pfeiffer. "The AME 2012 atomic mass evaluation (II). Tables, graphs and references". In: *Chin. Phys.* C36.12 (2012).

[83] T. Nilsson, G. Nyman and K. Riisager. "Halo-nuclei at ISOLDE". In: *Hyperfine Interact.* 129.1 (2000), pp. 67–81. DOI: 10.1023/A:1012678320350.

[84] D. R. Tilley, J. H. Kelley, J. L. Godwin, D. J. Millener, J. E. Purcell, C. G. Sheu and H. R. Weller. "Energy levels of light nuclei". In: *Nucl. Phys. A* 745.3–4 (2004), pp. 155–362. DOI: 10.1016/j.nuclphysa.2004.09.059.

[85] D. J. Millener, D. E. Alburger, E. K. Warburton and D. H. Wilkinson. "Decay scheme of ^{11}Be". In: *Phys. Rev. C* 26 (3 Sept. 1982), pp. 1167–1185. DOI: 10.1103/PhysRevC.26.1167.

[86] A. Becerril, M. J. G. Borge, J. A. Briz, O. Forstner, L. M. Fraile, H. O. U. Fynbo, J. S. Johansen, B. Jonson, G. T. Koldste, K. L. Laursen, M. V. Lund, T. Nilsson, G. Nyman, K. Riisager, P. Steier and O. Tengblad. "Search for beta-delayed protons from ^{11}Be". In: *Proposal to the ISOLDE and Neutron Time-of-Flight Committee* (2012).

[87] S. Bubin and L. Adamowicz. "Calculations of the ground states of BeH and BeH+ without the Born-Oppenheimer approximation". In: *J. Chem. Phys.* 126.21, 214305 (2007). DOI: 10.1063/1.2736699.

[88] C. A. Diget, F. C. Barker, M. J. G. Borge, J. Cederkäll, V. N. Fedosseev, L. M. Fraile, B. R. Fulton, H. O. U. Fynbo, H. B. Jeppesen, B. Jonson, U. Köster, M. Meister, T. Nilsson, G. Nyman, Y. Prezado, K. Riisager, S. Rinta-Antila, O. Tengblad, M. Turrion, K. Wilhelmsen and J. Äystö. "Properties of the ^{12}C 10 MeV state determined through -decay". In: *Nucl. Phys. A* 760.1 (2005), pp. 3–18. DOI: 10.1016/j.nuclphysa.2005.05.159.

[89] Z. Kohley, T. Baumann, D. Bazin, G. Christian, P. A. DeYoung, J. E. Finck, N. Frank, M. Jones, E. Lunderberg, B. Luther, S. Mosby, T. Nagi, J. K. Smith, J. Snyder, A. Spyrou and M. Thoennessen. "Study of Two-Neutron Radioactivity in the Decay of ^{26}O". In: *Phys. Rev. Lett.* 110 (15 Apr. 2013), p. 152501. DOI: 10.1103/PhysRevLett.110.152501.

[90] E. Lunderberg, P. A. DeYoung, Z. Kohley, H. Attanayake, T. Baumann, D. Bazin, G. Christian, D. Divaratne, S. M. Grimes, A. Haagsma, J. E. Finck, N. Frank, B. Luther, S. Mosby, T. Nagi, G. F. Peaslee, A. Schiller, J. Snyder, A. Spyrou, M. J. Strongman and M. Thoennessen. "Evidence for the Ground-State Resonance of ^{26}O". In: *Phys. Rev. Lett.* 108 (14 Apr. 2012), p. 142503. DOI: 10.1103/PhysRevLett.108.142503.

[91] C. R. Hoffman, T. Baumann, D. Bazin, J. Brown, G. Christian, P. A. DeYoung, J. E. Finck, N. Frank, J. Hinnefeld, R. Howes, P. Mears, E. Mosby, S. Mosby, J. Reith, B. Rizzo, W. F. Rogers, G. Peaslee, W. A. Peters, A. Schiller, M. J. Scott, S. L. Tabor, M. Thoennessen, P. J. Voss and T. Williams. "Determination of the $N = 16$ Shell Closure at the Oxygen Drip Line". In: *Phys. Rev. Lett.* 100 (15 Apr. 2008), p. 152502. DOI: 10.1103/PhysRevLett.100.152502.

[92] L. V. Grigorenko, I. G. Mukha, C. Scheidenberger and M. V. Zhukov. "Two-neutron radioactivity and four-nucleon emission from exotic nuclei". In: *Phys. Rev. C* 84 (2 Aug. 2011), p. 021303. DOI: 10.1103/PhysRevC.84.021303.

[93] J. D. Bowman, A. M. Poskanzer, R. G. Korteling and G. W. Butler. "Detection of neutron-excess isotopes of low-Z elements produced in high-energy nuclear reactions". In: *Phys. Rev. C* 9 (3 Mar. 1974), pp. 836–851. DOI: 10.1103/PhysRevC.9.836.

[94] M. Langevin, E. Quiniou, M. Bernas, J. Galin, J. C. Jacmart, F. Naulin, F. Pougheon, R. Anne, C. Détraz, D. Guerreau, D. Guillemaud-Mueller and A. C. Mueller. "Production of neutron-rich nuclei at the limits of particles stability by fragmentation of 44 MeV/u ^{40}Ar projectiles". In: *Phys. Lett.* B150.1–3 (1985), pp. 71–74. DOI: 10.1016/0370-2693(85)90140-6.

[95] H. G. Bohlen, B. Gebauer, T. Kirchner, M. von Luckepetsch, W. von Oertzen, A. N. Ostrowski, C. Seyfert, T. Stolla, M. Wilpert, T. Wilpert, S. M. Grimes, T. Massey, R. Kalpakchieva, Y. E. Penionzhkevich, D. V. Alexandrov, I. Mukha, A. A. Ogoblin and C. Detraz. "Study of light neutron-rich nuclei with ^{14}C-induced reactions". In: *Nucl. Phys.* A583 (1995), pp. 775–782. DOI: 10.1016/0375-9474(94)00757-E.

[96] R. A. Kryger, A. Azhari, J. Brown, J. Caggiano, M. Hellström, J. H. Kelley, B. M. Sherrill, M. Steiner and M. Thoennessen. "Upper limit of the lifetime of B-16". In: *Phys. Rev. C* 53 (1996), pp. 1971–1973. DOI: 10.1103/PhysRevC.53.1971.

[97] R. Kalpakchieva, H. G. Bohlen, W. von Oertzen, B. Gebauer, M. von Lucke-Petsch, T. N. Massey, A. N. Ostrowski, T. Stolla, M. Wilpert and T. Wilpert. "Spectroscopy of ^{13}B, ^{14}B, ^{15}B and ^{16}B using multi-nucleon transfer reactions". In: *Eur. Phys. J. A* 7.4 (2000), pp. 451–461. DOI: 10.1007/PL00013641.

[98] J.-L. Lecouey, N. A. Orr, F. M. Marqués, N. L. Achouri, J.-C. Angélique, B. A. Brown, F. Carstoiu, W. N. Catford, N. M. Clarke, M. Freer, B. R. Fulton, S. Grévy, F. Hanappe, K. L. Jones, M. Labiche, R. C. Lemmon, A. Ninane, E. Sauvan, K. M. Spohr and L. Stuttgé. "Single-Proton Removal Reaction Study of B-16". In: *Phys. Lett.* B672 (2009), pp. 6–11. DOI: 10.1016/j.physletb.2008.12.053. arXiv: 0802.4225 [nucl-ex].

[99] A. Spyrou, T. Baumann, D. Bazin, G. Blanchon, A. Bonaccorso, E. Breitbach, J. Brown, G. Christian, A. DeLine, P. A. DeYoung, J. E. Finck, N. Frank, S. Mosby, W. A. Peters, A. Russel, A. Schiller, M. J. Strongman and M. Thoennessen. "First evidence for a virtual B-18 ground state". In: *Phys. Lett.* B683 (2010), pp. 129–133.

[100] E. K. Warburton and B. A. Brown. "Effective interactions for the $p-s-d$ nuclear shell-model space". In: *Phys. Rev. C* 46 (3 Sept. 1992), pp. 923–944. DOI: 10.1103/PhysRevC.46.923.

[101] M. Dufour and P. Descouvemont. "Low-lying resonances in the B-16 nucleus". In: *Phys. Lett.* B696 (2011), pp. 237–240. DOI: 10.1016/j.physletb.2010.12.032.

[102] M. R. Mumpower, R. Surman, G. C. McLaughlin and A. Aprahamian. "The impact of individual nuclear properties on r-process nucleosynthesis". In: *Progress in Particle and Nuclear Physics* 86 (2016), pp. 86–126. DOI: 10.1016/j.ppnp.2015.09.001.

[103] M. R. Mumpower, R. Surman, G. C. McLaughlin and A. Aprahamian. "Corrigendum to"The impact of individual nuclear properties on r-process nucleosynthesis" [J. Prog. Part. Nucl. Phys. 86C (2015)]". In: *Progress in Particle and Nuclear Physics* 87 (2016), p. 116. DOI: 10.1016/j.ppnp.2015.12.002.

[104] C. A. Bertulani and T. Kajino. "Frontiers in nuclear astrophysics". In: *Progress in Particle and Nuclear Physics* 89 (2016), pp. 56–100. DOI: 10.1016/j.ppnp.2016.04.001.

[105] J. José. *Stellar Explosions Hydrodynamics and Nucleosynthesis*. Ed. by M. Birkinshaw, J. Silk and G. Fuller. Taylor and Francis Group, 2016.

[106] H. Schatz. "Trends in nuclear astrophysics". In: *J. Phys. G* 43.6 (2016), p. 064001. URL: http://stacks.iop.org/0954-3899/43/i=6/a=064001.

[107] M. Terasawa, K. Sumiyoshi, T. Kajino, G. J. Mathews and I. Tanihata. "New Nuclear Reaction Flow during r-Process Nucleosynthesis in Supernovae: Critical Role of light, neutron-rich Nuclei". In: *Astrophys. J* 562.1 (2001), p. 470. URL: http://stacks.iop.org/0004-637X/562/i=1/a=470.

[108] T. Sasaqui, T. Kajino, G. J. Mathews, K. Otsuki and T. Nakamura. "Sensitivity of r-Process Nucleosynthesis to Light-Element Nuclear Reactions". In: *Astrophys. J* 634.2 (2005), p. 1173. URL: http://stacks.iop.org/0004-637X/634/i=2/a=1173.

[109] T. Rauscher, J. H. Applegate, J. J. Cowan, F. K. Thielemann and M. Wiescher. "Production of Heavy Elements in Inhomogeneous Cosmologies". In: *Astrophys. J* 429.2, 1 (July 1994), pp. 499–530. DOI: 10.1086/174339.

[110] G. Baur, C. A. Bertulani and H. Rebel. "Coulomb dissociation as a source of information on radiative capture processes of astrophysical interest". In: *Nucl. Phys. A* 458.1 (1986), pp. 188–204. DOI: 10.1016/0375-9474(86)90290-3.

[111] J. Benlliure. "Isospin effects in fragmentation reactions". In: *EPJ Web of Conferences*. Vol. 88. 00028. EDP Sciences, 2015. DOI: 10.1051/epjconf/20158800028.

[112] M. Eliasson, A. Furufors, L. Johansson, T. Lundqvist and J. Roderus. *Where is the Detection Limit?* B. Sc. Thesis. Chalmers University of Technology. June 2016.

Acknowledgements

I would like to sincerely thank those people listed below.

Who	Why
Thomas Nilsson	for supervision and support.
Andreas Heinz	for supervision and support.
Håkan Johansson	for development of useful tools, commenting manuscripts, and other help.
Björn Jonsson	for commenting manuscripts and answering physics questions.
Simon Lindberg	finally another PhD student at Chalmers working on the same things.
The subatomic physics group	for a good working environment and interesting discussions.
The R^3B collaboration	for experiments, discussions, detector development.
The MAGISOL collaboration	for nice experiments at CERN-ISOLDE.
Family	for support.
Friends	for support.
Fabian	for sharing our lives.

A. Experimental determination of the trigger efficiency

A.1 Background

In order to calculate cross sections it is necessary to determine the amount of incoming and of reacted ions[1]. These two types of events do not necessarily lead to the same signatures in our detectors, as reactions usually produce additional particles. In Table A.1, the different signatures leading to triggers (trigger patterns) are summarized. The use of these hardware triggers is necessary to selectively decrease the amount of collected data, so that all events of interest are collected, but without saturating the data acquisition with events of less interest (e.g. no nuclear reaction). Events were no nuclear reaction takes place are the most likely, and even though enough of them need to be collected, not all of them are needed. Therefore some trigger patterns (1, 2 and 6) are downscaled[2]. This downscale needs to be compensated for during the analysis, meaning that events cannot be blindly mixed, since the trigger pattern needs to be selected[3]. The trigger patterns 3 and 7 are for calibration purposes only and are essentially switched off, except during data collection for calibration. This leaves three reaction triggers which are not downscaled: one indicating neutrons in the neutron detector, one signaling protons in the proton arm, and one indicating energy deposit in the Crystal Ball (protons, neutrons or γ-rays). Note that these reaction trigger patterns all contain also the requirements which are needed for the fragment trigger pattern (2).
The amount of incoming ions is usually determined from the amount of unre-

[1] More precisely: the number of ions that underwent the reaction of which the cross section is to be determined.

[2] That a trigger is downscaled by a factor d means that only every d^{th} event is stored to disc.

[3] Of course, one can add data from different trigger patterns, but care must be taken to avoid double-counting and the potentially different downscales need to be compensated for.

raw triggger / trigger pattern	POSIROLU	LAND mult. 2	TFW mult. 2	DTF mult. 2	XB sum	S8	PIX mask	beam on	early pile up	late trigger
1 Min. Bias	x	-	-	-	-	-	-	x	-	-
2 Fragment	x	-	x	-	-	-	-	x	a	-
3 FRS S8	-	-	-	-	-	x	-	-	-	-
4 XB sum	x	-	x	-	x	-	-	x	a	a
5 Proton	x	-	x	x	-	x	-	x	a	-
6 GB - pileup	x	-	-	-	-	-	-	x	a	-
7 Pix	x	-	-	-	-	-	x	x	-	-
8 Neutron	x	x	x	-	-	-	-	x	a	-

Table A.1: Table indicating which raw triggers have to be present in order to generate the trigger patterns for inspill data collection. The generated trigger patterns are listed in the first column and the needed raw triggers are indicated by an “x” in the respective columns. An “a” indicates an anti-coincidence requirement and “-” indicates no requirement. The highlighted rows show the triggers of interest in this discussion.

acted ions, compensated for the reaction probability in the target. This choice has the advantage that losses due to acceptance in the fragment arm of the setup do not need to be considered, when comparing incoming to reacted beam, as they, determined in this way, affect both the unreacted and the reacted ions, thus trigger pattern 2 is the natural choice to select these events.
The choice of the trigger pattern to select the events in which the reaction of interest took place, depends of course on the reaction. In the present case of (1pxn) removal cross sections, with no further selection than a reconstructed fragment, in principle the fragment trigger pattern would have been sufficient. Unfortunately that was downscaled by a factor of 64, rendering the statistics of the reacted beam, collected with this trigger pattern, too small.
Instead, it turns out that the XB trigger pattern (4) triggered in most of the reactions. Therefore the trigger pattern 4 was selected for choosing the reacted beam events.
In order to be able to calculate the cross sections, the trigger efficiency of the trigger pattern 4 in comparison to trigger pattern 2 needs to be determined.

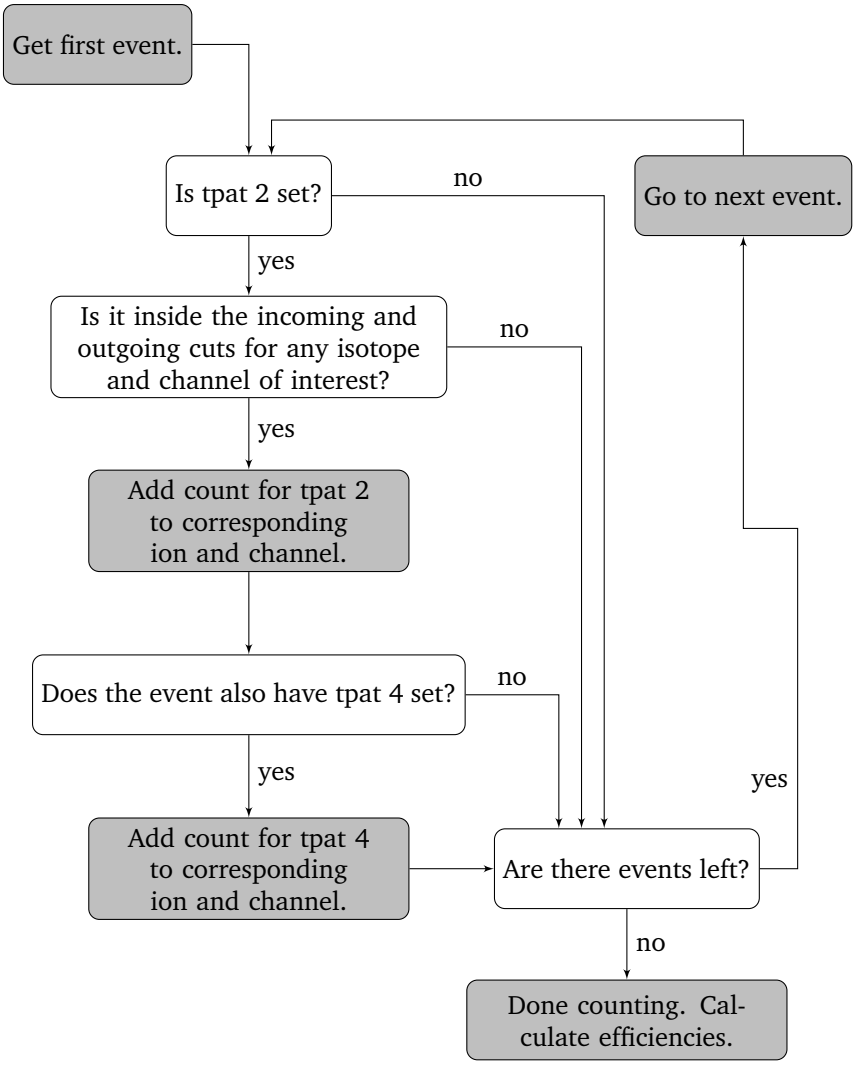

Figure A.1: Flowchart illustrating the event filtering flow to determine the trigger efficiency. Trigger pattern is abbreviated with tpat. For details see text.

A.2 Determining the trigger efficiency

The trigger pattern 4 (XB) is equal to the trigger pattern 2 (Fragment) plus a trigger from the Crystal Ball[4], c.f. Table A.1. In order to determine the trigger efficiency of trigger pattern 4 it is, for our purposes, sufficient to determine the relative trigger efficiency of trigger pattern 4 versus trigger pattern 2.
The procedure is the following: count for each isotope and each reaction channel how many events are tagged with trigger pattern 2 (*count1*), and how many of these are also tagged with trigger pattern 4 (*count2*). Events must be counted, since the low statistics does not allow for fits. The flowchart given in Fig. A.1 illustrates the counting procedure. The formulation "inside incoming and outgoing cuts" refers to the fragment identification as described in Sec. 4.3, plus a condition on the outgoing mass to be at maximum 2σ from an outgoing mass of interest, to ensure a unique selection. The relative trigger efficiency is calculated by dividing *count2* by *count1*.
In this way the trigger efficiency for different reaction channels for different isotopes can be determined and compared, as shown in Fig. A.2. In order to cope with the large statistical fluctuations, the determined efficiency as a function of the amount of removed neutrons, averaged over all ions is shown in Fig. A.3, together with the average of all reaction channels. From these two figures, I conclude that the trigger efficiency of the XB trigger pattern relative to the fragment trigger pattern does not, inside the statistical uncertainties, depend on ion or reaction channel[5], and that correcting for one average trigger efficiency is reasonable. Averaging the results for the different reaction channels, weighted according to their statistical uncertainties yields a trigger efficiency for the XB trigger pattern of (85.3 ± 2.5) % of the fragment trigger pattern (as also shown in Fig. A.3).

[4]The reader might have noticed the "late trigger" anti-coincidence too. This is needed to block raw triggers from the Crystal Ball as they sometimes arrive too late.

[5]This conclusion is restricted to the investigated ions and reaction channels.

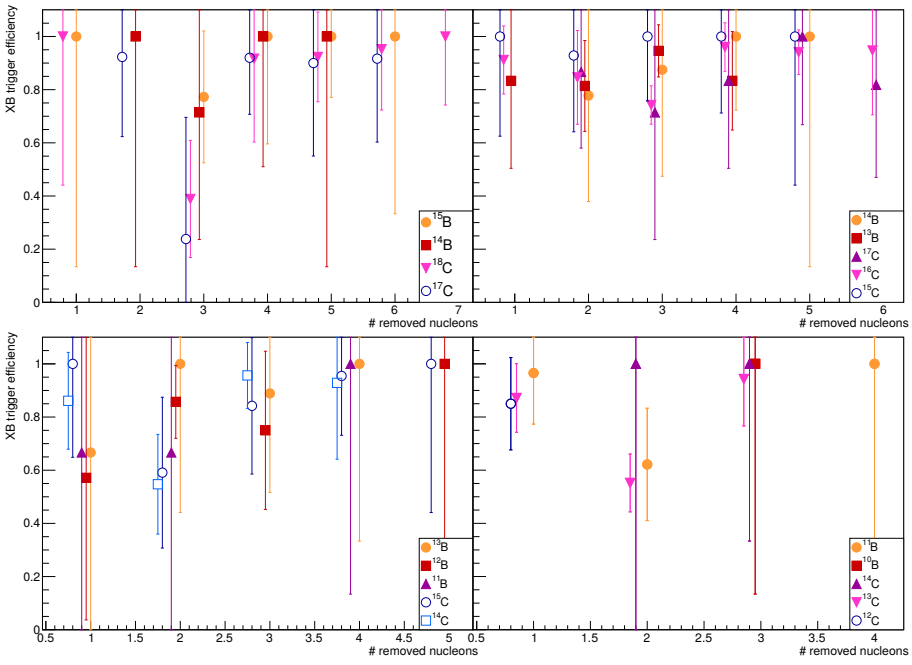

Figure A.2: Overview of the trigger efficiencies calculated for different reaction channels and incoming ions. The different data points are offset in (negative) x-direction to improve readability, the number of removed nucleons is in these cases the next larger integer. The plots show data collected with different accelerator settings. The error bars are purely statistical.

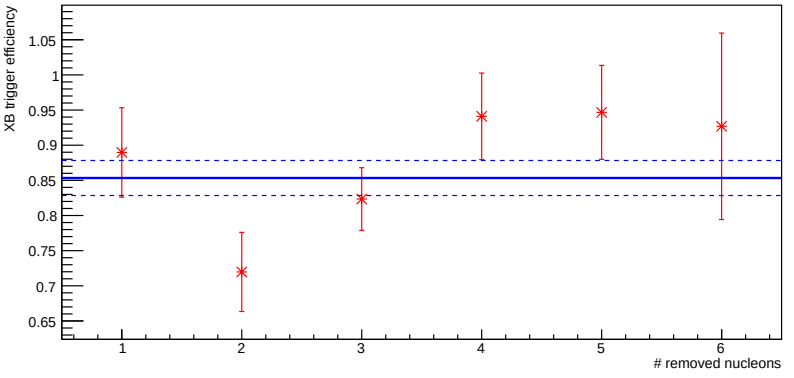

Figure A.3: Averaged trigger efficiency as a function of removed nucleons (red stars). The total average is shown as (blue) line, with 1σ uncertainty indicated by the dashed (blue) lines. All errors are statistical errors only.

B. How to find the best fit ABRABLA07 calculation

The goal is to determine which ABRABLA07 calculation best describes the experimental data, depending on the f_{EE} (excitation energy multiplication factor) used in the ABRABLA07 calculation. This is determined for each incoming ion separately, using all its available channels of 1pxn removal, with $0 \leq x \leq 5$, together.

A typical example of the evolution of the calculated cross sections with changing f_{EE} in comparison to the data is shown in Fig. B.1. This figure hints at the difficulties: the overall trend of the cross sections should be reproduced, but the overall magnitudes as well — and in some nuclei these are conflicting requirements.

The natural choice is to determine a χ^2 of the calculation in comparison to the data. For that, all contributions to uncertainties are needed. The statistical uncertainty of the experimental data we have at hand, and the systematic uncertainty is estimated to (at least) 5 %. The square root of the sum the squares of those two uncertainties for a specific ion and reaction channel is called ${}^{\sigma}_{\mathrm{x}}\Delta_{i,k}$. This, and the further notation is summarized in Table B.1, and will not be explained in the text. Indices to the bottom left of a symbol mark its properties, and indices to the top left mark the quantity the symbol relates to, while indices to the bottom right indicate what the variable depends on. The upper right side of a symbol is reserved for its exponent. This gives ${}^{\text{quantity}}_{\text{property}}S^{\text{exponent}}_{\text{variables}}$ in short[1]. I use this notation, because it facilitates possible re-implementation in computer code.

Aside from the statistical uncertainty of the model calculation which was rendered negligible by simulating a sufficient number of events for all channels of interest, there is no knowledge of the theoretical uncertainty or error of the model. This needs to be estimated. For that we assume that the uncertainty of the model calculation is the average difference between calculated and exper-

[1] If you need an example: ${}^{\sigma}_{\mathrm{x}}\Delta_{i,k}$ is the error (Δ) of the experimental (x) cross section (σ) depending on ion (i) and removal channel (k).

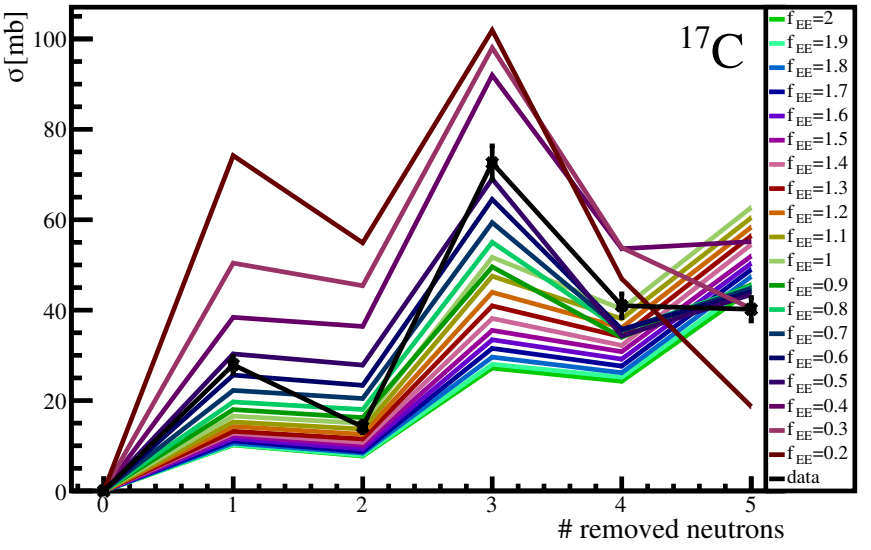

Figure B.1: Cross section versus the number of removed neutrons in a 1pxn removal reaction from ^{17}C. The black crosses with error bars (statistical only) show the experimental data. The different colours represent the different excitation energy multiplication factors (f_{EE}) used in the ABRABLA07 calculations.

imental data for the the best fit calculation. This would require the knowledge of which calculation fits best, which we aim at deriving. Therefore we approximate the uncertainty in two steps. We first calculate a preliminary χ^2 ($_{\mathrm{p}}\chi^2_{i,f}$) without taking the theoretical uncertainty into account:

$$ {}_{\mathrm{p}}\chi^2_{i,f} = \frac{1}{K}\sum_{k}^{K} \frac{({}_{\mathrm{x}}\sigma_{i,k} - {}_{\mathrm{t}}\sigma_{i,k,f})^2}{{}^{\sigma}_{\mathrm{x}}\Delta_{i,k}{}^2}. \tag{B.1} $$

For each ion we can find the minimal $_{\mathrm{p}}\chi^2_{i,f}$, and from that the best f_{EE} ($^{\wedge}_{\mathrm{p}}\chi^2 f_i$). From the difference between the calculation with $^{\wedge}_{\mathrm{p}}\chi^2 f_i$ and the data, we derive the theoretical uncertainty. First the relative theoretical uncertainty of the cross section is estimated as:

$$ {}^{\sigma}_{\mathrm{t}}\delta_i = \frac{1}{M}\sqrt{\sum_{k\in\mathscr{M}} \frac{(|{}_{\mathrm{x}}\sigma_{i,k} - {}^{\wedge\mathrm{f}}_{\mathrm{t}}\sigma_{i,k}| - {}^{\sigma}_{\mathrm{x}}\Delta_{i,k})^2}{{}_{\mathrm{x}}\sigma_{i,k}{}^2}} \tag{B.2} $$

$$ \mathscr{M} = \{\forall k : |{}_{\mathrm{x}}\sigma_{i,k} - {}^{\wedge\mathrm{f}}_{\mathrm{t}}\sigma_{i,k}| > {}^{\sigma}_{\mathrm{x}}\Delta_{i,k}\}, $$

Symbol	Description
Δ	Uncertainty
δ	Relative uncertainty
σ	Cross section
f	f_{EE}, excitation energy multiplication factor
i	Incoming ion
k	Reaction channel
M	Total number of elements in $\mathscr{M}$
$\mathscr{M}$	set of k: $\mathscr{M} = \{\forall k : \lvert {}_{\mathrm{x}}\sigma_{i,k} - {}^{\wedge\mathrm{f}}_{\mathrm{t}}\sigma_{i,k}\rvert > {}^{\sigma}_{\mathrm{x}}\Delta_{i,k}\}$
K	Total number of reaction channels (of one isotpe)
x	Marks an experimental value.
t	Marks a theoretical value (ABRABLA07).
p	Marks a preliminary value.
d	Marks a final value.
$\wedge$	Marks a minimized value.

Table B.1: Description of the symbols used for describing the minimization procedure. Indices to the left of a symbol mark its properties, while indices at the bottom right indicate what the variable depends on. The upper right side of a symbol is reserved for its exponent. This notation was chosen to facilitate re-implementation in computer code.

from the data points were the difference between calculation and data is larger than the experimental uncertainty for each ion. To obtain a total theoretical uncertainty, ${}^{\sigma}_{\mathrm{t}}\Delta_{i,k,f}$, the relative uncertainty is multiplied with the cross section:

$$ {}^{\sigma}_{\mathrm{t}}\Delta_{i,k,f} = {}^{\sigma}_{\mathrm{t}}\delta_i \cdot {}_{\mathrm{t}}\sigma_{i,k,f}. \tag{B.3} $$

This is used for a final calculation of the χ^2 (${}_{\mathrm{d}}\chi^2_{i,f}$) which takes the theoretical uncertainty into account:

$$ {}_{\mathrm{d}}\chi^2_{i,f} = \frac{1}{K}\sum_{k}^{K} \frac{({}_{\mathrm{x}}\sigma_{i,k} - {}_{\mathrm{t}}\sigma_{i,k,f})^2}{{}^{\sigma}_{\mathrm{x}}\Delta_{i,k}{}^2 + {}^{\sigma}_{\mathrm{t}}\Delta_{i,k,f}{}^2}. \tag{B.4} $$

From that we can find the f_{EE} for which the χ^2 is minimal, i.e. ${}^{\wedge\chi^2}_{\mathrm{d}}f_i$. We would also like to have a measure of how robust this result is, basically depending on how steep the ${}_{\mathrm{d}}\chi^2_{i,f}$ rises around ${}^{\wedge\chi^2}_{\mathrm{d}}f_i$. The uncertainty of the ${}_{\mathrm{d}}\chi^2_{i,f}$ is estimated as:

$$ {}^{\wedge\chi^2}_{\mathrm{d}}\Delta_i = 2 \cdot \sqrt{{}^{\wedge}_{\mathrm{d}}\chi^2_i}. \tag{B.5} $$

To estimate the uncertainty of ${}^{\wedge\chi^2}_{\mathrm{d}}f_i$ we select all f_{EE} which correspond to a ${}_{\mathrm{d}}\chi^2_{i,f}$ such that ${}_{\leq}\chi^2_{i,f}\,{}^{\wedge}_{\mathrm{d}}\chi^2_i \pm {}^{\wedge\chi^2}_{\mathrm{d}}\Delta_i$. The largest difference between the selected

f_{EE} and ${}^{\wedge}\chi^2_{\mathrm{d}} f_i$ is determined for $f > {}^{\wedge}\chi^2_{\mathrm{d}} f_i$ and $f < {}^{\wedge}\chi^2_{\mathrm{d}} f_i$ respectively. The average of these two differences is considered the uncertainty of ${}^{\wedge}\chi^2_{\mathrm{d}} f_i$.